




**Link overlap influences opinion dynamics on multiplex networks of Ashkin-Teller spins**Cook Hyun Kim,<sup>1</sup> Minjae Jo ,<sup>1</sup> J. S. Lee,<sup>2</sup> G. Bianconi ,<sup>3,4</sup> and B. Kahng <sup>5</sup><sup>1</sup>*CCSS, CTP and Department of Physics and Astronomy, Seoul National University, Seoul 08826, Korea*<sup>2</sup>*School of Physics, Korea Institute for Advanced Study, Seoul 02455, Korea*<sup>3</sup>*School of Mathematical Sciences, Queen Mary University of London, E1 4GF, London, United Kingdom*<sup>4</sup>*Alan Turing Institute, The British Library, NW1 2DB, London, United Kingdom*<sup>5</sup>*Center for Complex Systems, KI of Grid Modernization, Korea Institute of Energy Technology, Naju, Jeonnam 58217, Korea*

(Received 19 June 2021; revised 20 October 2021; accepted 22 November 2021; published 9 December 2021)

Consider a multiplex network formed by two layers indicating social interactions: the first layer is a friendship network and the second layer is a network of business relations. In this duplex network each pair of individuals can be connected in different ways: they can be connected by a friendship but not connected by a business relation, they can be connected by a business relation without being friends, or they can be simultaneously friends and in a business relation. In the latter case we say that the links in different layers overlap. These three types of connections are called multilinks and the multidegree indicates the sum of multilinks of a given type that are incident to a given node. Previous opinion models on multilayer networks have mostly neglected the effect of link overlap. Here we show that link overlap can have important effects in the formation of a majority opinion. Indeed, the formation of a majority opinion can be significantly influenced by the statistical properties of multilinks, and in particular by the multidegree distribution. To quantitatively address this problem, we study a simple spin model, called the Ashkin-Teller model, including two-body and four-body interactions between nodes in different layers. Here we fully investigate the rich phase diagram of this model which includes a large variety of phase transitions. Indeed, the phase diagram of the model displays continuous, discontinuous, and hybrid phase transitions, and successive jumps of the order parameters within the Baxter phase.

DOI: [10.1103/PhysRevE.104.064304](https://doi.org/10.1103/PhysRevE.104.064304)**I. INTRODUCTION**

Over the past two decades, network theory [1–5] has provided the pivotal framework for characterizing the interplay between graph structures and dynamics of complex systems. Recently, multilayer networks [6–10] are attracting considerable scientific interest. These network of networks are able to integrate information on various types of links characterizing complex systems where interactions have different nature and connotation. Therefore, they provide a useful perspective for analyzing complex social, transportation, or biological systems [11–15], etc. Multilayer networks not only have rich correlated structures [16–19] that encode more information than a single layer, but also contain various dynamical processes that are strongly affected by the multiplexity of the network. These dynamical processes include percolation [7,17,20–24], diffusion [25,26], epidemic spreading [27–29], and game theory [30,31], etc.

Multiplex networks are a special class of multilayer network consisting of a set of nodes connected by  $M$  different types of links. Each network consisting of a given type of link interaction forms one of the  $M$  layers of a multiplex network.

Most social networks are multiplex. In fact, social ties have different connotations possibly indicating friends, colleagues, acquaintances and family relations, etc. Moreover, in the modern society, online social interactions can occur between different online social networks such as Twitter, Facebook,

LinkedIn, etc. The vast majority of data on multiplex social networks display a significant link overlap [11,12,16]. This property indicates that a significant fraction of pair of nodes can be connected at the same time by more than one type of interaction. For example, it might occur that a colleague is also a friend or that two individuals might be connected at the same time on Facebook and Twitter.

The opinion dynamics on social multiplex networks have been investigated recently using spin models such as the voter models [32–36], election models [37], and Hamiltonian spin systems [38]. The observed dynamics on social multiplex networks cannot be reduced to the dynamics on a single social aggregated network that treats all the interactions of the multiplex network on an equal footing. In adaptive voter models, an absorbing and shattered fragmentation transition [33,34] occurs in which one layer can be fragmented into two clusters, each one reaching consensus on a different opinion, whereas the other layer remains connected in one cluster. In election models, the competing campaigns of two parties can give rise to election outcomes in which both parties have a large electorate [37]. Additionally, the party investing more in building a connected network of supporters is more likely to win the election [37]. In studies of the opinion dynamics on multiplex networks, where different opinions can be spread across different layers, an important question is whether each node maintains coherent behavior, that is, has a similar opinion in all the layers. A spin opinion model displaying a

coherence–incoherence transition was numerically investigated recently [38]. Spins are coupled within each layer to represent the interaction between one node and its neighbors on a given topic and also across layers to represent the tendency of each node to take a coherent opinion on all the topics.

Another spin model, which illustrates opinion dynamics in social networks due to the influence of interdependence between different social communities, is the Ashkin-Teller model [39]. It was studied on scale-free (SF) network in which the degree distribution follows power law and an analytical approach revealed that a rich phase diagram including the critical end point was obtained [40]. It was considered on a duplex network with identical topology; however, the most realistic multiplex network [7] can be the case in which the layers of the bilayer network are distinct and the amount of overlap is tunable.

Here our goal is to investigate to what extent link overlap affects the opinion dynamics defined on multiplex networks and whether link overlap favors coherent opinions.

We consider a duplex network formed by two layers where a two-state opinion dynamics takes place. For example, one could consider a voting model for the city council and for the national parliament. For each vote, nodes can be influenced by a different set of nodes. In the previous example, the first layer indicates the network influencing the city council vote, the second layer indicates the network determining the national vote. The link overlap has a clear effect on this opinion dynamics by coupling the two layers. In fact if two nodes are connected in both layers it is natural to assume that the simultaneous alignment of the opinions in both layers must be favored by the dynamics. This considerations allow us to model the opinion dynamics in presence of link overlap, with a spin Hamiltonian model that is a variation of the Ashkin-Teller (AT) model [39,40] that we call  $g$ -AT model.

The model contains two species of Ising spins, the  $s$ -spin and  $\sigma$ -spin, with each species of spin located on a single layer of the duplex network. The duplex network is a maximum entropy duplex network with given multidegree distribution [16] and as such it is very suitable to modulate the role of overlapping multilinks. In particular, we assume that nonoverlapping multilinks and overlapping multilinks have a SF multidegree distribution characterized by a different power-law exponent. Here we provide a complete analytical mean-field solution to this model and we reveal the complex phase diagram of the model. We show that favoring the simultaneous alignment of the opinions of nodes connected in both layers provides a simple mechanism to generate coherence of opinions.

This paper is organized as follows: We introduce the Hamiltonian of the  $g$ -AT model and the duplex network topology under study in Sec II. In Sec. III we derive the free-energy density using the mean-field approximation and then self-consistency equations for the order parameters by minimizing the free-energy density. Next, from these self-consistency equations, we obtain the susceptibilities. In Secs. IV and V, we obtain rich phase diagrams in which different phases in the parameter space are delimited by lines, indicating phase transitions (PTs) of different order. Note that the phase diagrams are richer than those of the original AT model on SF networks [40], because the links are classified into two types:

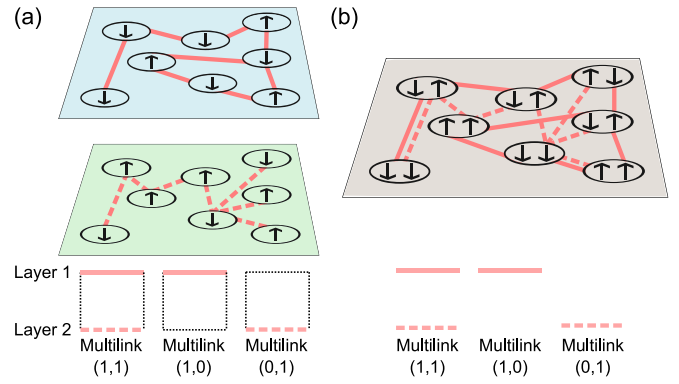


FIG. 1. (a) The  $g$ -AT model on a duplex network: two species ( $s_i, \sigma_i$ ) of Ising spins describe, respectively, the opinion of node  $i$  in layers 1 and 2. Each pair of nodes of the duplex network can be connected by a different type of multilink: multilinks (1,1) connect pair of nodes in both layers 1 and 2; multilinks (1,0) and (0,1) connect pair of nodes only in layer 1 and only in layer 2, respectively. Therefore, multilinks (1,1) describe overlapping links while multilinks (1,0) and (0,1) describe nonoverlapping links. The model can be also interpreted as a model on a colored network in which nodes are an associated pair of spin and the interactions between each pair of nodes can be distinguished in multilinks (1, 1), (1, 0), and (0,1) (b).

nonoverlapping and overlapping links. Finally, we summarize the results in Sec. VI.

## II. MODEL AND FORMALISM

We consider a duplex network formed by  $N$  nodes  $i \in \{1, 2, \dots, N\}$ . Every pair of nodes ( $i, j$ ) of the duplex network can be connected in multiplex ways. To indicate these different type of connections we use multilinks introduced in Ref. [16]. In particular, we say that a pair of nodes ( $i, j$ ) is connected by a multilink (1,0) if they are only connected in layer 1, they are connected by a multilink (0,1) if they are only connected in layer 2, and they are connected by a multilink (1,1) if they are connected in both layers. Every pair of nodes can be connected only by one type of multilink, alternatively they can be unconnected in both layers (see Fig. 1). We call multiadjacency matrices the matrices of elements  $A_{ij}^{(1,0)}$ ,  $A_{ij}^{(0,1)}$ , and  $A_{ij}^{(1,1)}$ , indicating whether or not the pair of nodes ( $i, j$ ) is connected by a multilink (1,0), a multilink (0,1), and a multilink (1,1), respectively. This general duplex network topology includes link overlap captured by the multilinks (1,1). The presence of such multilinks has been observed in a variety of social networks [11,12]. Here and in the following we indicate with multidegrees  $k_i^{(1,0)}$ ,  $k_i^{(0,1)}$ , and  $k_i^{(1,1)}$  the numbers of multilinks incident to the node  $i$ , i.e.,

$$k_i^{(1,0)} = \sum_{j=1}^N A_{ij}^{(1,0)}, k_i^{(0,1)} = \sum_{j=1}^N A_{ij}^{(0,1)},$$

$$k_i^{(1,1)} = \sum_{j=1}^N A_{ij}^{(1,1)}. \quad (1)$$

On such a duplex network, we consider the  $g$ -AT model that describes opinion dynamics and takes into account the

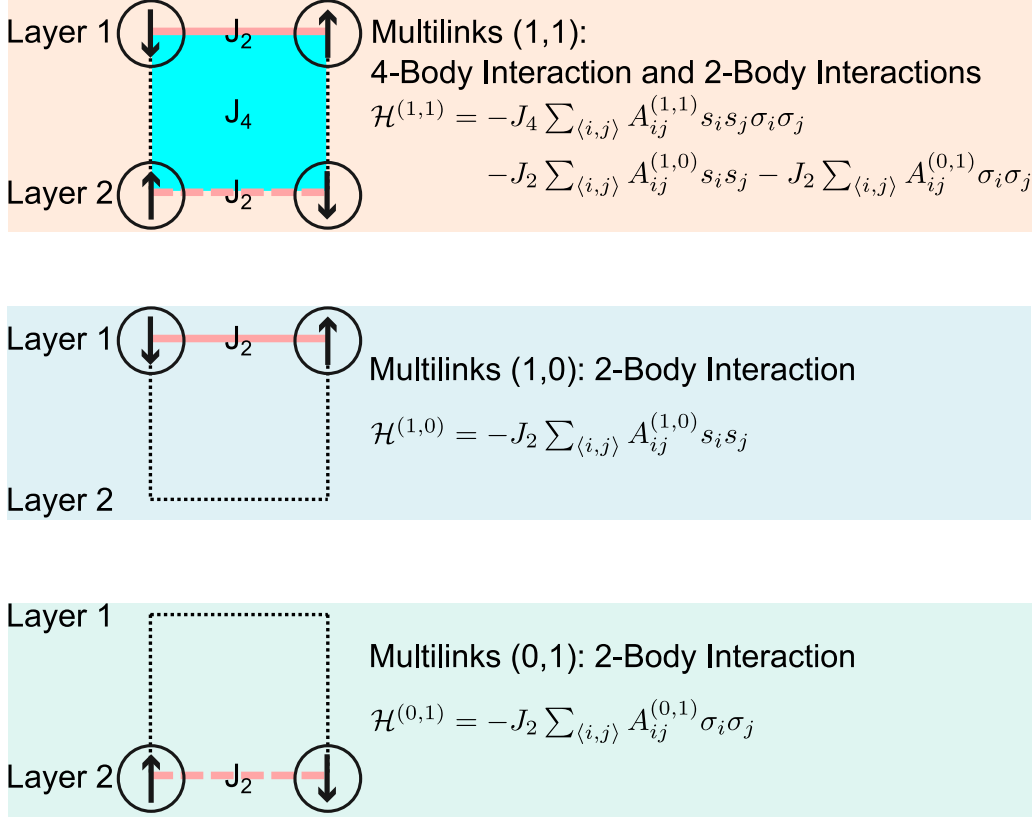


FIG. 2. The  $g$ -AT model is an Hamiltonian model combining two-body and four-body interactions. The four-body interactions characterizes the interactions between the spins of species  $s_i$  and  $\sigma_i$  connected by a multilink (1,1). The two-body interactions characterize the coupling between spins of a given species (either the spins  $s_i$  or the spins  $\sigma_i$ ) connected by either a multilink (1,0) or (0,1).

role that link overlap has on this dynamics. We consider two species of Ising spins  $s_i$  and  $\sigma_i$  associated with the dynamics on layers 1 and 2, respectively. The two spins take values  $s_i \in \{-1, 1\}$  and  $\sigma_i \in \{-1, 1\}$ . These spin variables are interacting via two-body interactions and four-body interactions (see Fig. 2). In particular, for each multilink (1,0) connecting node  $i$  to node  $j$ , we have a two-body Ising interaction between the spins  $s_i$  and  $s_j$  with coupling constant  $J_2$ . Similarly, for each multilink (0,1) connecting node  $i$  to node  $j$ , we have a two-body Ising interaction between the spins  $\sigma_i$  and  $\sigma_j$  with coupling constant  $J_2$ . For each multilink (1,1) instead we consider a combination of two-body and four-body interactions. The two-body interactions tend to align spins associated to the same layer with coupling constant  $J_2$ . The four-body interactions couples instead the four spins  $s_i$ ,  $s_j$ ,  $\sigma_i$ , and  $\sigma_j$ , and is modulated by a coupling constant  $J_4$ . In particular, the Hamiltonian of the  $g$ -AT model without an external magnetic field is expressed as the sum of three terms,

$$\mathcal{H}_o = \mathcal{H}^{(1,0)} + \mathcal{H}^{(0,1)} + \mathcal{H}^{(1,1)}, \quad (2)$$

where

$$\begin{aligned} \mathcal{H}^{(1,0)} &= -J_2 \sum_{(i,j)} A_{ij}^{(1,0)} s_i s_j, \\ \mathcal{H}^{(0,1)} &= -J_2 \sum_{(i,j)} A_{ij}^{(0,1)} \sigma_i \sigma_j, \end{aligned}$$

$$\begin{aligned} \mathcal{H}^{(1,1)} &= -J_4 \sum_{(i,j)} A_{ij}^{(1,1)} s_i s_j \sigma_i \sigma_j \\ &\quad - J_2 \sum_{(i,j)} A_{ij}^{(1,0)} s_i s_j - J_2 \sum_{(i,j)} A_{ij}^{(0,1)} \sigma_i \sigma_j, \end{aligned} \quad (3)$$

with the pairs of connected nodes  $\langle i, j \rangle$ . Alternatively, the Hamiltonian  $\mathcal{H}_o$  of the  $g$ -AT model without an external magnetic field can be expressed more concisely as

$$-\beta \mathcal{H}_o = K_2 \sum_{(i,j)} \mathbf{s}_i^T \mathbf{A}_{ij} \mathbf{s}_j, \quad (4)$$

where  $\mathbf{s}_i = (s_i, \sigma_i, s_i \sigma_i)^T$ , and the matrix  $\mathbf{A}_{ij}$  is given by

$$\mathbf{A}_{ij} = \begin{pmatrix} A_{ij}^{(1,0)} + A_{ij}^{(1,1)} & 0 & 0 \\ 0 & A_{ij}^{(0,1)} + A_{ij}^{(1,1)} & 0 \\ 0 & 0 & x A_{ij}^{(1,1)} \end{pmatrix}, \quad (5)$$

where  $x \equiv J_4/J_2$ . Moreover,  $\beta = 1/k_B T$ , where  $k_B$  is the Boltzmann constant,  $T$  is the temperature, and  $K_2 \equiv \beta J_2$  with coupling constant  $J_2$ . For later discussion, we define similarly  $K_4 \equiv \beta J_4$ .

Here, we investigate the critical properties of this model on a maximum entropy duplex network model with given multidegree distribution [16]. To distinguish between multilinks (1,1) which imply link overlap and the other multilinks (1,0) and (0,1) which do not, we assume for simplicity that each node  $i$  of the multiplex network has the same multidegree

(1,0) and multidegree (0,1), and we indicate the multidegree of nonoverlapping multilinks and of overlapping multilinks as

$$\begin{aligned} k_i^{(1,0)} &= k_i^{(0,1)} = k_{n,i}, \\ k_i^{(1,1)} &= k_{o,i}, \end{aligned} \quad (6)$$

where the subscript  $n$  of  $k_{n,i}$  indicates and the subscript  $o$  of  $k_{o,i}$  indicates *nonoverlap* and *overlapping* multilinks, respectively. We assume that the degree distributions corresponding to *overlapping* and *nonoverlapping* multilinks are power-law functions with exponents  $\lambda_o$  and  $\lambda_n$ , respectively. The degree distribution is shortly written as

$$P_d(k_a) \sim k_a^{-\lambda_a}, \quad (7)$$

where  $a \in \{o, n\}$ .

In the considered ensemble of duplex networks [16] a pair of nodes  $(i, j)$  is connected by (1,0) multilinks with probability  $p_{ij}^{(1,0)}$ , by (0,1) multilinks with probability  $p_{ij}^{(0,1)}$ , and by (1,1) multilinks with probability  $p_{ij}^{(1,1)}$ , where we have

$$\begin{aligned} p_{ij}^{(1,0)} &= \frac{k_i^{(1,0)} k_j^{(1,0)}}{\langle k^{(1,0)} \rangle N}, \\ p_{ij}^{(0,1)} &= \frac{k_i^{(0,1)} k_j^{(0,1)}}{\langle k^{(0,1)} \rangle N}, \\ p_{ij}^{(1,1)} &= \frac{k_i^{(1,1)} k_j^{(1,1)}}{\langle k^{(1,1)} \rangle N}, \end{aligned} \quad (8)$$

with  $\langle k^{(1,0)} \rangle$ ,  $\langle k^{(0,1)} \rangle$ , and  $\langle k^{(1,1)} \rangle$  being the average multidegrees. Indeed, these marginal probabilities are obtained in the maximum entropy ensemble with given multidegree distribution as long as the degree distribution display the structural cutoff. Here, we consider the thermodynamic limit ( $N \rightarrow \infty$ ) and power-law exponents greater than 3, so that the effect of structural cutoff can be ignored.

The phase diagram of this model will be affected by the topology of multiplex network and the strength of the inter-layer interaction. This can be studied as a function of three parameters,  $\lambda_n$ ,  $\lambda_o$ , and  $x \equiv J_4/J_2$ . The ratio  $x$  quantifies the degree strength of four-body interaction with respect to the strength of two-body interactions for between nodes linked by multilinks (1,1).

The original AT model [40] comprises two species of Ising spins,  $s_i$  and  $\sigma_i$ , locating at each node  $i$  on a monolayer network. The original AT model can be thus recovered as a limit case of the  $g$ -AT model in absence of nonoverlapping multilinks and when  $x = 1$  (i.e.,  $J_4 = J_2$ ). Indeed, in this limit we recover the Hamiltonian for the original AT model given by

$$\mathcal{H} = -J_2 \sum_{\langle ij \rangle} (s_i s_j + \sigma_i \sigma_j) - J_2 \sum_{\langle ij \rangle} s_i s_j \sigma_i \sigma_j, \quad (9)$$

which can be rewritten in the form of the four-state Potts model as

$$\mathcal{H} = -4J_2 \sum_{\langle ij \rangle} (\delta(q_i, q_j) - 1/4), \quad (10)$$

where  $q_i$  is a Potts spin with value 0,1,2 or 3 at node  $i$  and  $\delta(q_i, q_j) = 1$  for  $q_i = q_j$ , and zero otherwise [41]. Since the

nonoverlapping multilinks are absent, the phase diagram of the original model is a function of a single power-law exponent  $\lambda$  of the degree distribution. Clearly this power-law exponent correspond to the power-law exponent  $\lambda_o$  of overlapping links of the  $g$ -AT model.

### III. MEAN-FIELD SOLUTION

To obtain the Landau free energy, we calculate the Hamiltonian in Eq. (4) by the mean-field approximation. We first take the local order parameters  $\mathbf{m}_i = (m_i^s, m_i^\sigma, m_i^{s\sigma})^T$ , whose components are defined as  $m_i^s = \langle s_i \rangle$ ,  $m_i^\sigma = \langle \sigma_i \rangle$ , and  $m_i^{s\sigma} = \langle s_i \sigma_i \rangle$ . Here  $\langle \dots \rangle$  is the ensemble average of a given quantity. Next, we expand each spin variable with respect to the respective local order parameter as  $\mathbf{s}_i = (m_i^s + \delta m_i^s, m_i^\sigma + \delta m_i^\sigma, m_i^{s\sigma} + \delta m_i^{s\sigma})^T$ . We can neglect the higher-order terms in  $\delta m_i^s$ ,  $\delta m_i^\sigma$ , and  $\delta m_i^{s\sigma}$  because the magnitude of these terms is very small compared to that of the local order parameter. The mean-field Hamiltonian  $\mathcal{H}_{\text{mf}}$  can be written as

$$-\beta \mathcal{H}_{\text{mf}} \simeq -K_2 \sum_{i,j} \mathbf{m}_i^T \mathbf{A}_{ij} \mathbf{m}_j + K_2 \sum_{i,j} \mathbf{m}_i^T \mathbf{A}_{ij} (\mathbf{s}_j + \sigma_j). \quad (11)$$

Then, we obtain the mean-field Landau free energy  $\mathcal{F}$ , which is given by

$$\begin{aligned} \beta \mathcal{F} &= -\ln Z \\ &= -\ln \sum_{\{s_i, \sigma_i\}} e^{-\beta \mathcal{H}_{\text{mf}}} \simeq -\sum_i \ln Z_i + K_2 \sum_{i,j} \mathbf{m}_i^T \mathbf{A}_{ij} \mathbf{m}_j, \end{aligned} \quad (12)$$

where

$$Z_i = 4[C_i(s)C_i(\sigma)C_i(s\sigma) + S_i(s)S_i(\sigma)S_i(s\sigma)], \quad (13)$$

with

$$C_i(s) \equiv \cosh \left( \sum_{j \in \text{nn}(i)} K_2 m_j^s \right), \quad S_i(s) \equiv \sinh \left( \sum_{j \in \text{nn}(i)} K_2 m_j^s \right). \quad (14)$$

Here  $\sum_{j \in \text{nn}(i)}$  indicates that the summation runs over all the nearest neighbors  $j$  of node  $i$  for each of the three types of links.

Next, we use the annealed approximation to perform the summation:

$$\begin{aligned} \sum_{\langle i,j \rangle} A_{ij}^{(1,0)} \mathcal{A}_{ij} &\rightarrow \frac{1}{2} \sum_{i,j} p_{ij}^{(1,0)} \mathcal{A}_{ij}, \\ \sum_{\langle i,j \rangle} A_{ij}^{(0,1)} \mathcal{A}_{ij} &\rightarrow \frac{1}{2} \sum_{i,j} p_{ij}^{(0,1)} \mathcal{A}_{ij}, \quad \text{and} \\ \sum_{\langle i,j \rangle} A_{ij}^{(1,1)} \mathcal{A}_{ij} &\rightarrow \frac{1}{2} \sum_{i,j} p_{ij}^{(1,1)} \mathcal{A}_{ij}, \end{aligned} \quad (15)$$

where  $\mathcal{A}_{ij}$  is a given function of  $i$  and  $j$  and  $p_{ij}^{(1,0)}$ ,  $p_{ij}^{(0,1)}$  and  $p_{ij}^{(1,1)}$  are defined in Eq. (8).

We define a global order magnetization for  $s$  spin as

$$m_s^{(1,0)} = \frac{\sum_i k_i^{(1,0)} m_i^s}{N \langle k^{(1,0)} \rangle} \quad \text{and} \quad m_s^{(1,1)} = \frac{\sum_i k_i^{(1,1)} m_i^s}{N \langle k^{(1,1)} \rangle}, \quad (16)$$



where  $m_i^s$  is the local order parameter for  $s$  spin. We introduce global order parameters for  $\sigma$  and  $s\sigma$  spins similarly. Then, we set that  $M \equiv m_{s\sigma}^{(1,1)}$ .

Since the considered duplex network ensemble has the same multidegree distribution of the nonoverlapping multi-links we can set

$$m_s^{(1,0)} = m_\sigma^{(0,1)} \equiv m_n, \quad m_s^{(1,1)} = m_\sigma^{(1,1)} \equiv m_o. \quad (17)$$

The three order parameters are now denoted as  $m_o$ ,  $m_n$ , and  $M$ -magnetization, respectively. Applying the annealed approximation, we rewrite the free-energy density ( $f \equiv \beta\mathcal{F}/N$ ) in terms of the order parameters  $m_n$ ,  $m_o$ , and  $M$ . The free-energy density  $f$  is given by

$$\begin{aligned} f \simeq & K_2 m_n^2 \langle k_n \rangle + K_2 m_o^2 \langle k_o \rangle + \frac{1}{2} K_4 M^2 \langle k_o \rangle \\ & - 2 \int_{k_{\min}^n}^{\infty} \int_{k_{\min}^o}^{\infty} dk_n dk_o P_d(k_n) P_d(k_o) \\ & \times \ln [\cosh (K_2 (m_n k_n + m_o k_o))] \\ & - \int_{k_{\min}^o}^{\infty} dk_o P_d(k_o) \ln [\cosh (K_4 M k_o)] - \mathcal{B}_1, \end{aligned} \quad (18)$$

where  $K_4 = \beta J_4$  with coupling constant  $J_4$  and

$$\mathcal{B}_1 = \int_{k_{\min}^n}^{\infty} \int_{k_{\min}^o}^{\infty} dk_n dk_o P_d(k_n) P_d(k_o) \ln (1 + \mathcal{T}_2^2 \mathcal{T}_4), \quad (19)$$

with

$$\mathcal{T}_2 \equiv \tanh (K_2 (m_n k_n + m_o k_o)), \quad \mathcal{T}_4 \equiv \tanh (K_4 M k_o). \quad (20)$$

Minimizing the free-energy density  $f$ ,  $\partial f / \partial m_a = 0$  and  $\partial f / \partial M = 0$ , we obtain the following self-consistency relations:

$$m_a \langle k_a \rangle = \int_{k_{\min}^n}^{\infty} \int_{k_{\min}^o}^{\infty} dk_n dk_o P_d(k_n) P_d(k_o) \frac{\mathcal{T}_2 (1 + \mathcal{T}_4)}{1 + \mathcal{T}_2^2 \mathcal{T}_4} k_a, \quad (21)$$

where  $a \in \{o, n\}$ , and

$$M \langle k_o \rangle = \int_{k_{\min}^n}^{\infty} \int_{k_{\min}^o}^{\infty} dk_n dk_o P_d(k_n) P_d(k_o) \frac{\mathcal{T}_4 + \mathcal{T}_2^2}{1 + \mathcal{T}_2^2 \mathcal{T}_4} k_o. \quad (22)$$

The self-consistency relations Eqs. (21) and (22) admit three solutions, corresponding to the paramagnetic phase ( $m_a = 0, M = 0$ ), the Baxter phase ( $m_a > 0, M > 0$ ), and the  $\langle \sigma s \rangle$  phase ( $m_a = 0, M > 0$ ).

To obtain the susceptibility, we also consider a Hamiltonian including an external magnetic field, given by

$$-\beta\mathcal{H} = -\beta\mathcal{H}_o + \sum_i \mathbf{H}_i^T \mathbf{s}_i, \quad (23)$$

where  $\mathbf{H}_i = (k_{o,i} H_o + k_{n,i} H_n, k_{o,i} H_o + k_{n,i} H_n, k_{o,i} H_4)^T$ .  $H_a$  is the external magnetic field applied to  $s$  and  $\sigma$  spins in proportion to the multidegree  $k_a$  and  $H_4$  is another external magnetic field applied to  $s\sigma$  spins in proportion to degree  $k_o$ . Minimizing the free-energy density, we obtain the self-consistency equations for magnetizations with respect to external magnetic fields:

$$-\frac{\partial f}{\partial H_a} = m_a \langle k_a \rangle, \quad -\frac{\partial f}{\partial H_4} = M \langle k_o \rangle. \quad (24)$$

These self-consistency equations can be obtained by substituting  $K_2 m_a k_a$  and  $K_4 M k_o$  with  $(K_2 m_a + H_a) k_a$  and  $(K_4 M + H_4) k_o$ , respectively, in Eqs. (18), (19), (21), and (22) (see Appendix A). The susceptibilities are calculated using the following relations:

$$\chi_a \equiv \left. \frac{\partial m_a}{\partial H_a} \right|_{H_a, H_4 \rightarrow 0}, \quad \chi_M \equiv \left. \frac{\partial M}{\partial H_4} \right|_{H_a, H_4 \rightarrow 0}. \quad (25)$$

Using the above relations, the susceptibilities  $\chi$  can be obtained as follows:

$$\chi_a = \frac{\mathcal{A}_{aa} + \mathcal{A}_{a\bar{a}} K_2 \partial m_{\bar{a}} / \partial H_a + \mathcal{A}_{aM} K_4 \partial M / \partial H_a}{\langle k_a \rangle - K_2 \mathcal{A}_{aa}}, \quad (26)$$

$$\chi_M = \frac{\mathcal{A}_{MM} + \mathcal{A}_{M_o} K_2 \partial m_o / \partial H_4 + \mathcal{A}_{M_n} K_2 \partial m_n / \partial H_4}{\langle k_o \rangle - K_4 \mathcal{A}_{MM}}, \quad (27)$$

where  $a \in \{n, o\}$  and  $\bar{a} \in \{n, o\}$  with  $a$  different from  $\bar{a}$ . Here the  $\mathcal{A}$  terms are obtained as follows:

$$\begin{aligned} \mathcal{A}_{aa} &= \frac{\partial m_{a1}}{\partial H_a}, \quad \mathcal{A}_{a\bar{a}} = \frac{\partial m_{a1}}{\partial H_{\bar{a}}}, \quad \mathcal{A}_{aM} = \frac{\partial m_{a1}}{\partial H_4}, \\ \mathcal{A}_{Ma} &= \frac{\partial M_1}{\partial H_a}, \quad \text{and} \quad \mathcal{A}_{MM} = \frac{\partial M_1}{\partial H_4}. \end{aligned} \quad (28)$$

In Appendix B, we provide the extensive formulas for  $\mathcal{A}$ s in the limit  $H_a \rightarrow 0$  and  $H_4 \rightarrow 0$ , where  $m_{a1}$  and  $M_1$  are presented in intergral form in Eqs. (A2) and (A3).

## IV. PHASE DIAGRAM I: $J_4/J_2$ -DEPENDENCE

### A. Phases of the model

At equilibrium, the  $g$ -AT model admits three phases, paramagnetic phase, Baxter phase, and  $\langle \sigma s \rangle$  phase, depending on  $\lambda_n, \lambda_o, x = J_4/J_2$ , and  $T$ .

(i) The paramagnetic phase is characterized by the order parameters  $m_a = \langle s \rangle = \langle \sigma \rangle = 0, M = \langle \sigma s \rangle = 0$ . This is the characteristic phase found in the high-temperature region, where the stochastic element of the dynamics is dominant. This phase corresponds to an equilibrium configuration in which there is no majority opinion in either layer ( $m_a = 0$ ), and each node has a random and uncorrelated opinion in the two different layers ( $M = 0$ ). Therefore, this is the phase entirely dominated by noise.

(ii) The Baxter phase is characterized by the order parameters  $m_a = \langle s \rangle = \langle \sigma \rangle > 0$ , and  $M = \langle \sigma s \rangle > 0$ . This is the phase in which we observe the formation of a majority opinion which is the same in both layers ( $m_a > 0$ ). Therefore, each node has coherent opinions in the two distinct layers ( $M > 0$ ).

(iii) The  $\langle \sigma s \rangle$  phase (Coherent phase) is characterized by the order parameters  $m_a = \langle s \rangle = \langle \sigma \rangle = 0$ , and  $M = \langle \sigma s \rangle > 0$ . This phase occurs for high temperature and when  $x = J_4/J_2$  is sufficiently high, in which the four-body interactions are stronger than the two-body interactions; therefore, each single node of the multiplex network tends to have the same opinion in both layers but these opinions are not yet aligned with the opinion of their neighbors. As a consequence there is no yet formation of a majority opinion in each layer (i.e.,  $m_a = 0$ ). Note that the term of  $\langle \sigma s \rangle$  phase originates from the original paper in physics [39]. To impose a meaning on the phase in the perspective of opinion formation, we call it Coherent phase hereafter.

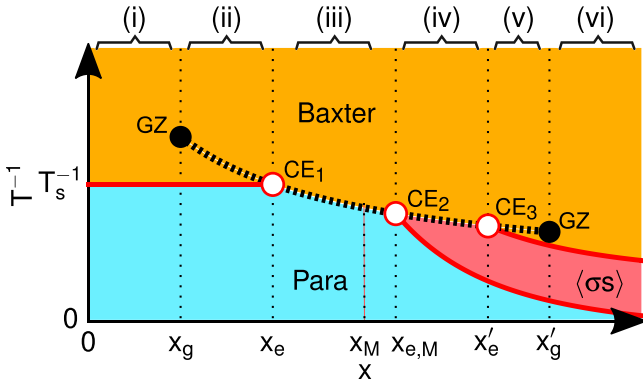


FIG. 3. Schematic phase diagram of the  $g$ -AT model for a given set of  $\lambda_n = 3.53$  and  $\lambda_o = 3.90$ . Solid and dotted curves represent continuous and discontinuous PTs, respectively. This phase diagram is mostly similar to the one of the original AT model [40].

### B. Classification of critical points and regions of the phase diagram

In the  $g$ -AT model the transitions between the phases Para, Baxter, and Coherent occurs as a function of the temperature  $T$  and very diverse and rich critical phenomena are observed. Indeed, the PTs can be continuous, discontinuous, hybrid, and in general we can observe more than one PT as the temperature  $T$  is lowered, while the other parameters are kept unchanged.

To be concrete we discuss here an exemplar phase diagram of the  $g$ -AT model in the parameter space  $[x, T^{-1}]$  (see Fig. 3). This phase diagram is obtained for the power-law exponents  $\lambda_n = 3.53$  and  $\lambda_o = 3.90$ . For this value of the power-law exponents, the phase diagram is similar to that of the original AT model [40] in the range  $\lambda_c < \lambda_o < 4$ , where  $\lambda_c \approx 3.503$  indicates the tricritical point (TP) of the original AT model [40]. In particular, we recall that in the original AT-model for  $\lambda_o > \lambda_c$ , the PT is of the first order; otherwise, it is of the second order [40,42,43]. Here we will describe in detail this phase diagram while the dependence of the phase diagram on the power-law exponents  $\lambda_n$  and  $\lambda_o$  will be treated in the next section.

In the phase diagram shown in Fig. 3, the three phases of the dynamics are denoted by Para ( $m_a = 0, M = 0$ ), Baxter phase ( $m_a > 0, M > 0$ ), and  $\langle\sigma s\rangle$  phase ( $m_a = 0, M > 0$ ). Dotted and solid lines represent discontinuous and continuous PTs, respectively. The critical temperature  $T_s$  denotes the temperature at which a second-order PT occurs from the Para phase to the Baxter phase. Note that  $T_s$  is independent on  $x = J_4/J_2$  for  $x < x_e$ .

The phase diagram has characteristic points denoted as GZs and CEs. We indicate with GZ a point at which the jump size (gap) of the order parameter becomes zero at each side of the dotted curve. We indicate with CE a critical endpoint, locating at the end of a continuous PT line, at which a line of first-order PT and a line of discontinuity of the order parameter merge. We will show that a mixed-order (or hybrid) transition occurs at these CE points. There are two GZs and three CEs in Fig. 3. Their  $x$  positions are asymmetric.

In the phase diagram shown in Fig. 3 we distinguish six regions based on the ratio  $x = J_4/J_2$ :

(i) In region (i), as the temperature is lowered the system undergoes a continuous PT at  $T_s$  from the Para to the Baxter phase. Therefore, as the noise is reduced the system goes continuously from a phase with the absence of any order, to a state with a clear majority opinion which is the same in both layers. This transition is denoted as (i)-type PT.

(ii) In region (ii), a continuous PT occurs at  $T_s$  between the Para and the Baxter phase. As  $T$  is lowered further, a discontinuous jump of the order parameters  $m_a$  and  $M$  occurs subsequently at  $T_f$ , in which we observe a discontinuity in  $m_a$  and  $M$  between two nonzero values. This indicates that at  $T_f$ , there is a discontinuous increment in the fraction of nodes adopting the majority opinion. This transition is denoted as (ii)-type PT.

(iii) In region (iii), a discontinuous PT occurs at  $T_f$  between the Para and the Baxter phase. This implies that a majority opinion is formed abruptly in both layers. This transition is denoted as (iii)-type PT.

(iv) In region (iv), a continuous PT occurs between the Para and the Coherent phase at  $T_{s,M}$ . As  $T$  is decreased further, a discontinuous PT occurs at  $T_f$  from the Coherent phase to the Baxter phase. This implies that as the noise is reduced, at temperatures below the first continuous transition each single node tend to adopt a coherent opinion in both layers, and then when the temperature is further reduced a majority opinion is reached abruptly in both layers. These transitions are denoted as (iv)-type PT.

(v) In region (v), two continuous PTs occur successively: between the Para and the Coherent phase at  $T_{s,M}$  and between the Coherent and the Baxter phase at  $T'_s$ , respectively. Then as the temperature is decreased further, the order parameters  $m_a$  and  $M$  jumps at  $T_f$  from one finite value to another. These transitions are denoted as (v)-type PT.

(vi) In region (vi), two continuous PTs occur between the Para and the Coherent phase at  $T_{s,M}$  and between the Coherent and the Baxter phase at  $T'_s$ . These transitions are denoted as (vi)-type PT.

### C. Free-energy landscape for the $x$ -dependence of phase transitions

In this paragraph we will discuss the critical behavior of the  $g$ -AT model as a function of the parameter  $x = J_4/J_2$ .

The phase diagram of the  $g$ -AT model can be treated separately for  $x < x_M$  and  $x > x_M$ , where  $x_M$  indicates the characteristic ratio between  $J_4$  and  $J_2$ . For  $x < x_M$ , the  $J_2$  interactions are dominant, and  $O(m_a) \gg O(M)$  near the transition temperature. However, for  $x > x_M$ ,  $J_4$  interactions (interlayer interaction) become dominant and  $O(m_a) \ll O(M)$  near the transition temperature. Thus, the Coherent phase can emerge. For the original AT model,  $x_M = 1$ ; however, for the  $g$ -AT model,  $x_M$  depends on  $\lambda_n$  and  $\lambda_o$ .  $x_M$  locates between  $x_e$  and  $x_{e,M}$  in Fig. 3. Explicit formula to derive  $x_M$  will be presented in Eq. (D5).

The free-energy landscape determines the location and type of PTs with respect to  $x$ . Here we provide the discussion of the main results obtained by investigating the properties of the free-energy density illustrated by in Figs. 4 and 5 near  $T_s$ . We refer the interested reader to the exact formula of the free-energy density  $f$  given in Appendix D.

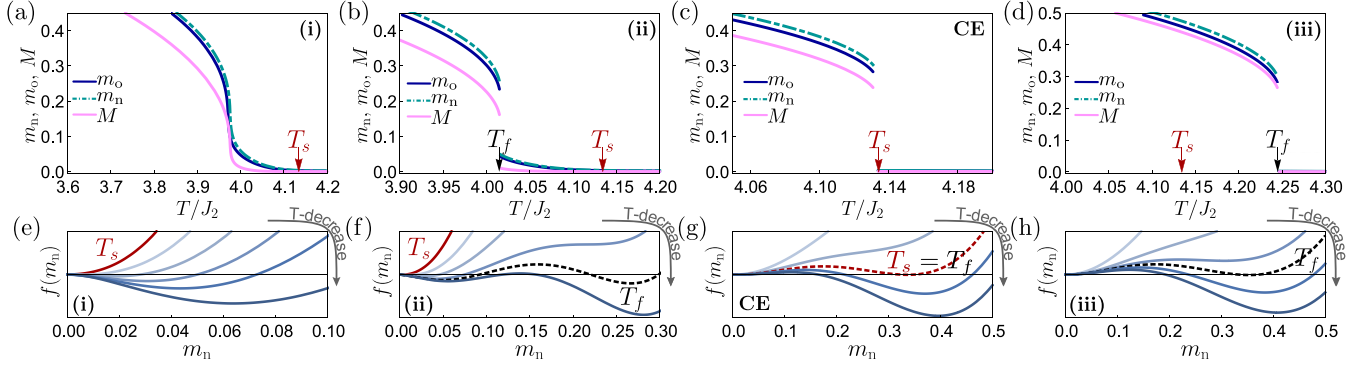


FIG. 4. (a)–(d) Plot of the order parameters  $m_a$  and  $M$  as a function of  $T/J_2$ . (e)–(h) Plot of the free-energy density landscape as a function of  $m_n$  for  $\lambda_n = 3.53$  and  $\lambda_o = 3.90$  and various interlayer interaction ratios:  $x = 1.30$  for (a) and (e);  $x = 1.40$  for (b) and (f);  $x = 1.62$  for (c) and (g); and  $x = 1.80$  for (d) and (h). The transition types are second order in region (i) for (a) and (e); successive continuous-discontinuous in region (ii) for (b) and (f); mixed-order at  $CE_1$  for (c) and (g); and discontinuous transition in region (iii) for (d) and (h).

### I. Case $0 < x < x_M$

In this paragraph we describe the critical behavior of the  $g$ -AT model for  $x < x_M$  including regions (i), (ii), and (iii), and a point  $CE_1$ . In region (i) a continuous PT occurs between the Para and the Baxter phase. Therefore, as the temperature is lowered, both  $m_a$  and  $M$  increase continuously for  $T < T_s$ .

Using Eqs. (D8) and (D11), we can obtain the critical behavior of the order parameters for  $T < T_s$ ,

$$m_a \sim (T_s - T)^{\beta_m} \quad \text{with} \quad \beta_m = \frac{1}{\lambda_{\min} - 3}, \quad (29)$$

$$M \sim (T_s - T)^{\beta_M} \quad \text{with} \quad \beta_M = \frac{\lambda_o - 2}{\lambda_{\min} - 3}, \quad (30)$$

where  $\lambda_{\min} = \min(\lambda_o, \lambda_n)$ . The specific heat scales as

$$C \sim (T_s - T)^{-\alpha} \quad \text{with} \quad \alpha = \frac{\lambda_{\min} - 5}{\lambda_{\min} - 3}. \quad (31)$$

The susceptibility diverges as (see Appendix E for the derivation)

$$\chi_a \sim \begin{cases} (T_s - T)^{-\gamma^-} & \text{with } \gamma^- = 1 \text{ for } T < T_s, \\ (T - T_s)^{-\gamma^+} & \text{with } \gamma^+ = 1 \text{ for } T > T_s. \end{cases} \quad (32)$$

Second, we observe that as  $x$  is increased but still remains less than  $x_M$ , a jump arises in the order parameters  $m_a$  and  $M$  in region (ii), observed for  $x_g < x < x_e$  in Fig. 3. We observe that the system undergoes a continuous second order transition at  $T_s$  between the Para and the Baxter phase characterized by the same critical exponents listed above. Moreover, as the temperature  $T$  is lowered further the system undergoes a sudden increase of the order parameter at  $T_f$ . Indeed, at  $T_f$  the free-energy density  $f$  displays a global minimum at a finite  $m_a$ , leading to the abrupt change of the order parameters [see Figs. 4(b) and 4(f)].

For  $x \rightarrow x_e$ , the temperature  $T_s$  becomes equal to  $T_f$ . Therefore, two global minima of  $f(m_a)$  occur at  $m_a = 0$  and  $m_a > 0$ , simultaneously. At this point, the second-order and the first-order transition lines merge. Therefore, the critical behavior

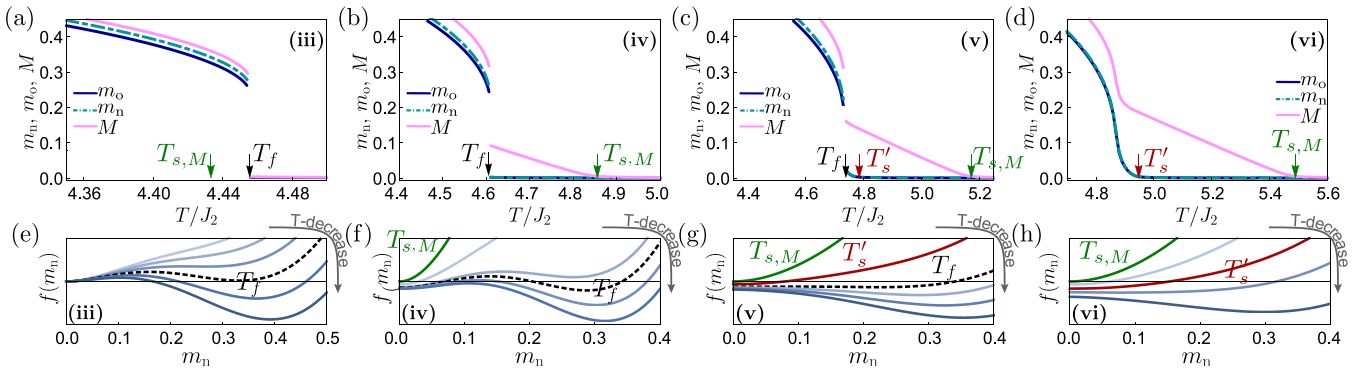


FIG. 5. (a)–(d) Plot of the order parameters  $m_a$  and  $M$  as a function of  $T/J_2$ . (e)–(h) Plot of the free-energy density landscape as a function of  $m_n$  for  $\lambda_n = 3.53$  and  $\lambda_o = 3.90$  and various interlayer interaction ratios:  $x = 2.10$  for panels (a) and (e);  $x = 2.30$  for panels (b) and (f);  $x = 2.45$  for panels (c) and (g); and  $x = 2.60$  for panels (d) and (h). The transition types are first-order in regime (iii) for panels (a) and (e); successive continuous-discontinuous in regime (iv) for panels (b) and (f); successive continuous-discontinuous in regime (v) for panels (c) and (g); and continuous transition in regime (vi) for panels (d) and (h).

appears, together with the jump of the order parameters  $m_a$  and  $M$  as illustrated in Figs. 4(c) and 4(g). This type of PT is referred to as a mixed-order (or hybrid) transition and this point is named as critical endpoint. However, the susceptibility  $\chi_m$  diverges at  $T_s^+$  as it appears in a continuous PT.

In region (iii), for  $x_e < x < x_M$ , a single discontinuous transition occurs at  $T_f$  between the Para and the Baxter phase. The critical behavior in this region is illustrated in Figs. 4(d) and 4(h).

## 2. Case $x \geq x_M$

Here, we consider the critical behavior of the  $g$ -AT model for  $x \geq x_M$  including the regions (iii), (iv), (v), and (vi) and two critical endpoints (CE<sub>2</sub>, CE<sub>3</sub>).

At  $x = x_M$  in region (iii), the free-energy densities  $f(m_a)$  and  $f(M)$  develop a local minimum at  $m_a^*$  larger than 0 and at a temperature  $T_f$  larger than  $T_{s,M}$  [Figs. 5(a) and 5(e)]. A discontinuous transition of  $m_a$  and  $M$  occurs between the Para and the Baxter phase at  $T_f$ . This phenomenology remains unchanged for  $x_M < x < x_{e,M}$ .

At  $x = x_{e,M}$ , the system is at the boundary between the regions (iii) and (iv), and we find the critical endpoint denoted as CE<sub>2</sub> in Fig. 3. At CE<sub>2</sub>, when the temperature  $T$  approaches  $T_{s,M}$  from below, i.e., when we explore the critical behavior for  $T \rightarrow T_{s,M}^-$ , we observe a discontinuity in the value of  $M$  from a nonzero value to zero, and thus the susceptibility does not diverge. However, when  $T$  approaches  $T_{s,M}$  from above, i.e., when we explore the critical behavior for  $T \rightarrow T_{s,M}^+$  even if  $M$  jumps suddenly and shows a behavior reminiscent of a first-order transition, the susceptibility  $\chi_M$  diverges. This is due to the fact that CE<sub>2</sub> is the endpoint of a line of second-order PTs between the Para and the Coherent phase. Thus, the magnetization  $M$  exhibits the properties of a mixed-order transition.

In region (iv), for  $x_{e,M} < x < x'_e$  we observe a continuous second order PT between the Para and the Coherent phase occurs at  $T_{s,M}$ . This is due to the behavior of the free-energy densities  $f(m)$  and  $f(M)$  which display a global minimum at  $m = 0$  and  $M = 0$  for  $T > T_{s,M}$ , while for  $T < T_{s,M}$ , a global minimum of  $f(M)$  appears at finite  $M > 0$ . The value of this global minimum of  $f(M)$  increases continuously as  $T$  is lowered. As  $T$  is decreased further and reaches  $T_f$ , new global minima of  $f(m_a)$  and  $f(M)$  appear at certain finite  $m_a$  and  $M$ . Thus, a first-order transition occurs and both order parameters  $m_a$  and  $M$  display a discontinuous jump. The critical behavior of the model in region (iv) is shown in Figs. 5(b) and 5(f).

At the boundary between the regions (iv) and (v), for  $x = x'_e$ , we observe the CE<sub>3</sub>, where the magnetization  $m_a$  changes discontinuously from 0 to a finite value at  $T_s'^-$ ; however, the susceptibility  $\chi_m$  diverges at  $T_s'^+$ . Thus, a mixed-order PT occurs at the CE<sub>3</sub>.

In region (v), for  $x'_e < x < x'_g$  as the temperature is gradually lowered we observe first a second-order PT between the Para and the Coherent phase at  $T_{s,M}$ , then we observe another second-order PT between the Coherent and the Baxter phase at  $T_s'$ . In addition to these two PTs we observe a jump of the order parameter  $m_a$  and  $M$  from nonzero values. This discontinuity can be obtained by studying the free-energy densities  $f(m_a)$  and  $f(M)$ . Indeed, when  $T > T_{s,M}$ , the global

minima of  $f(m_a)$  and  $f(M)$  remain at  $m_a = 0$  and  $M = 0$ . For  $T_s' < T < T_{s,M}$ , the global minimum of  $f(M)$  occurs at a finite  $M$ , which increases continuously as  $T$  is lowered gradually. Correspondingly, in this same range of temperatures, the global minimum of  $f(m_a)$  remains at still  $m_a = 0$ . As  $T$  gets below  $T_s'$ , a global minimum of  $f(m_a)$  emerges at a finite  $m_a > 0$  in a gradual way. Thus,  $m_a$  is finite, and a second-order PT occurs at  $T_s'$ . For this same range of temperature the global minimum of  $f(M)$  is achieved at an increasingly larger value of  $M$ . When  $T$  reaches  $T_f$ , new global minima of  $f(m_a)$  and  $f(M)$  emerge at finite  $m_a$  and  $M$ , which this minima being separated from the respective value of the free-energy minima obtained for  $T_f^+$ . Thus, a discontinuity occurs for the order parameter at  $T_f$ . These behaviors are schematically shown in Figs. 5(c) and 5(g).

In region (vi) corresponding to high values of  $x$  or  $x \rightarrow \infty$  two second-order PTs are observed. The first PT occurs between the Para and the Coherent phase at  $T_{s,M}$  and the second PT between the Coherent and the Baxter phase occurs at  $T_s'$ . These behaviors close to these two PTs are schematically shown in Figs. 5(d) and 5(h).

Using Eqs. (D19) and (D22), we can obtain the following critical behaviors for  $m_a$  and  $M$ :

$$m_a \sim (T_s' - T)^{\beta_m} \quad \text{with} \quad \beta_m = \frac{1}{\lambda_{\min} - 3}, \quad (33)$$

$$M \sim (T_{s,M} - T)^{\beta_M} \quad \text{with} \quad \beta_M = \frac{1}{\lambda_0 - 3}, \quad (34)$$

where  $\lambda_{\min} = \min(\lambda_0, \lambda_n)$ . Using these results, we obtain the specific heats, which scale as

$$C_m \sim (T_s' - T)^{-\alpha_m} \quad \text{with} \quad \alpha_m = \frac{\lambda_{\min} - 5}{\lambda_{\min} - 3}, \quad (35)$$

$$C_M \sim (T_{s,M} - T)^{-\alpha_M} \quad \text{with} \quad \alpha_M = \frac{\lambda_0 - 5}{\lambda_0 - 3}. \quad (36)$$

The susceptibilities behave as follows:

$$\chi_m \sim \begin{cases} (T - T_s')^{-\gamma_m^+} & \text{with } \gamma_m^+ = 1, \\ (T_s' - T)^{-\gamma_m^-} & \text{with } \gamma_m^- = 1, \end{cases} \quad (37)$$

and

$$\chi_M \sim \begin{cases} (T - T_{s,M})^{-\gamma_M^+} & \text{with } \gamma_M^+ = 1, \\ (T_{s,M} - T)^{-\gamma_M^-} & \text{with } \gamma_M^- = 1. \end{cases} \quad (38)$$

Detailed derivations of  $\chi_M$  and  $\chi_m$  near  $T_{s,M}$  and  $T_s'$ , respectively, are given in Appendix E.

## D. Anomalous scaling relations

The critical exponents of the continuous transition are listed in Table I for all ranges of  $x$ .

The scaling relation for  $m_a$  satisfies the conventional relation:

$$\alpha_m + 2\beta_m + \gamma_m = 2. \quad (39)$$

By contrast, the scaling relation for  $M$  shows an unusual behavior for  $x < x_M$ . The scaling relation for  $M$  does not hold



TABLE I. Critical exponents for  $3 < (\lambda_n, \lambda_o) < 4$ : Here,  $\alpha$  is the exponent of the specific heat,  $\beta_m$  ( $\beta_M$ ) is the exponent of the magnetization  $m_a$  ( $M$ ) at zero external magnetic field, and  $\gamma_m$  ( $\gamma_M$ ) is the exponent of the susceptibility for  $m_a$  ( $M$ )-magnetization near the transition temperature.

Range of $x$	$\alpha_m$	$\alpha_M$	$\beta_m$	$\beta_M$	$\gamma_{m\pm}$	$\gamma_{M\pm}$
$x = 0$	$\frac{\lambda_{\min}-5}{\lambda_{\min}-3}$	—	$\frac{1}{\lambda_{\min}-3}$	—	1	—
$0 < x < x_M$	$\frac{\lambda_{\min}-5}{\lambda_{\min}-3}$	$\frac{\lambda_{\min}-5}{\lambda_{\min}-3}$	$\frac{1}{\lambda_{\min}-3}$	$\frac{\lambda_o-2}{\lambda_o-3}$	1	0
$x = x_M$ ( $\lambda_n > \lambda_o$ )	$\frac{\lambda_o-5}{\lambda_o-3}$	$\frac{\lambda_o-5}{\lambda_o-3}$	$\frac{1}{\lambda_o-3}$	$\frac{1}{\lambda_o-3}$	1	1
$x = x_M$ ( $\lambda_n < \lambda_o$ )	$\frac{\lambda_n-5}{\lambda_n-3}$	$\frac{\lambda_o-5}{\lambda_o-3}$	$\frac{1}{\lambda_n-3}$	$\frac{1}{\lambda_o-3}$	1	1
$x > x_M$	$\frac{\lambda_{\min}-5}{\lambda_{\min}-3}$	$\frac{\lambda_o-5}{\lambda_o-3}$	$\frac{1}{\lambda_{\min}-3}$	$\frac{1}{\lambda_o-3}$	1	1

for  $x < x_M$  as

$$\alpha_M + 2\beta_M + \gamma_M = \begin{cases} 3 & \text{for } \lambda_n > \lambda_o, \\ 3 + 2\frac{\lambda_o - \lambda_n}{\lambda_n - 3} & \text{for } \lambda_n < \lambda_o. \end{cases} \quad (40)$$

Note that for the original AT model, the scaling relation for  $M$  is written as  $\alpha + 2\beta_M + \gamma_M = 3$ . This relation can be confirmed by setting  $\lambda_n = \lambda_o$  in the second equation of Eqs. (40).

## V. PHASE DIAGRAM II: $\lambda_a$ -DEPENDENCE

### A. General remarks

The  $g$ -AT model may be regarded as a combination of the original AT model on the network of overlapping links and two independent Ising models on the respective network of nonoverlapping links. To fully appreciate the general phase diagram of the  $g$ -AT model, let us recall three important results revealing the interplay between network structure and spin models, the Ising, Potts, and AT models.

The Ising model on a single SF network with power-law exponent  $\lambda$  exhibits a second-order PT at a finite temperature  $T_c \propto \langle k^2 \rangle / \langle k \rangle$  for  $\lambda > 3$  within the annealed approximation [44]. Thus, as  $\lambda$  increases,  $T_c$  decreases. Since the magnetization corresponds to the formation of a majority opinion, this implies that the larger the branching ratio  $\langle k^2 \rangle / \langle k \rangle$  of the network is, the easier it is for the network to display a majority opinion. In a single SF network, as the power-law exponent of degree distributions  $\lambda \rightarrow 3^+$  the branching ratio of the network increases as  $\langle k^2 \rangle / \langle k \rangle \simeq (\lambda - 2) / (\lambda - 3)$ . Therefore, this implies that tuning the power-law exponent  $\lambda$ , the network undergoes a topological change that affects the dynamics of spin model, in particular can modify the value of its critical temperature.

Consequently, we expect that the general phase diagram of the  $g$ -AT model will display a significant dependence on the pair of power-law exponents  $(\lambda_n, \lambda_o)$ . In particular, the relative value of  $\lambda_n$  with respect to  $\lambda_o$  allows to tune the relative influence of nonoverlapping multilinks with respect to overlapping multilinks. We have already seen that  $x = J_4/J_2$  modifies the phase diagram as it modulates the strength of the four-body interactions (mediated by overlapping multilinks) and the strength of two-body interactions (mediated by

nonoverlapping multilinks). We expect that the phase diagram depends on not only  $x$  but also the power-law exponents  $(\lambda_n, \lambda_o)$  significantly.

Let us recall that the original AT model can be recast in the Potts model with four states when we set  $x = J_4/J_2 = 1$  which display a tricritical PT when the power-law exponent  $\lambda_o = \lambda_c \approx 3.503$ . This implies that for  $\lambda_o > \lambda_c$ , the four state Potts model displays a first-order PT; otherwise, it displays a second-order PT [42]. From this observation we conclude that the phase diagram of the  $g$ -AT model is expected to be more rich around the values  $\lambda_n \simeq \lambda_c$  and  $\lambda_o \simeq \lambda_c$ .

### B. Additional regions of the general phase diagram

In Sec. IV we have described the  $x$ -dependence of the phase diagram of the  $g$ -AT model for a choice of power-law exponents  $(\lambda_n, \lambda_o) = (3.53, 3.90)$ . This phase diagram displays the PTs of types (i)–(vi), whose implications for opinion dynamics has been discussed in Sec. IV.

When we consider all possible values of the power-law exponents  $(\lambda_n, \lambda_o)$  we observe five more characteristic regions and lines, denoted as (vii)–(xi) in Fig. 6(b):

(1) In region (vii) of Figs. 6 and Fig. 7(a), two discontinuous behaviors occur successively as the temperature is lowered. This region can be divided into four subregions. These subregions are similar to (ii)–(v) regions in Fig. 7(b) but a discontinuous jump line additionally exists in a lower temperature region. The discontinuous jump line originates from the correlations between  $m_n$  of one layer and  $m_n$  or  $m_o$  of the other layer, whereas the other discontinuous jump lines in the interval  $[x_{g2}, x_e]$  and  $[x'_e, x'_{g1}]$  in a higher temperature region originates from the correlation between the same  $m_o$ s but on different layers.

In region (vii)<sub>1</sub> ( $x_{g2} < x < x_e$ ), a continuous PT between the Para and the Baxter phase occurs at  $T_s$  and two discontinuous jumps of the order parameters  $m_a$  and  $M$  occur successively as the temperature is lowered. As the noise (temperature) is reduced, the opinion dynamics exhibits first a continuous PT in which a majority opinion is formed in both layers, and spreads abruptly twice over a finite fraction of nodes in the multiplex network.

In region (vii)<sub>2</sub> ( $x_e < x < x_{e,M}$ ), as the temperature is lowered, a discontinuous PT between the Para and the Baxter phase occurs first, and subsequently a discontinuous jump of the order parameters  $m_a$  and  $M$  occurs in the same Baxter phase. Therefore, as the noise is reduced, the opinion dynamics has first a discontinuous PT in which a majority opinion is formed in both layers, and then we observe an additional jump in the magnetization as the majority opinion gets adopted by a larger fraction of nodes of the multiplex network.

In region (vii)<sub>3</sub> ( $x_{e,M} < x < x'_e$ ), a continuous PT occurs between the Para and the Coherent phase at  $T_{s,M}$ . As the temperature is decreased further, a discontinuous PT occurs at  $T_f$  from the Coherent phase to the Baxter phase and a discontinuous jump of the order parameters  $m_a$  and  $M$  occurs at  $T'_f$  successively. This implies that as the noise is reduced, at temperatures lower than  $T_{s,M}$ , each single node prefers to adopt a coherent opinion in both layers. As the temperature is further reduced, we observe a discontinuous PT in which majority opinion is formed in both layers, and then the majority

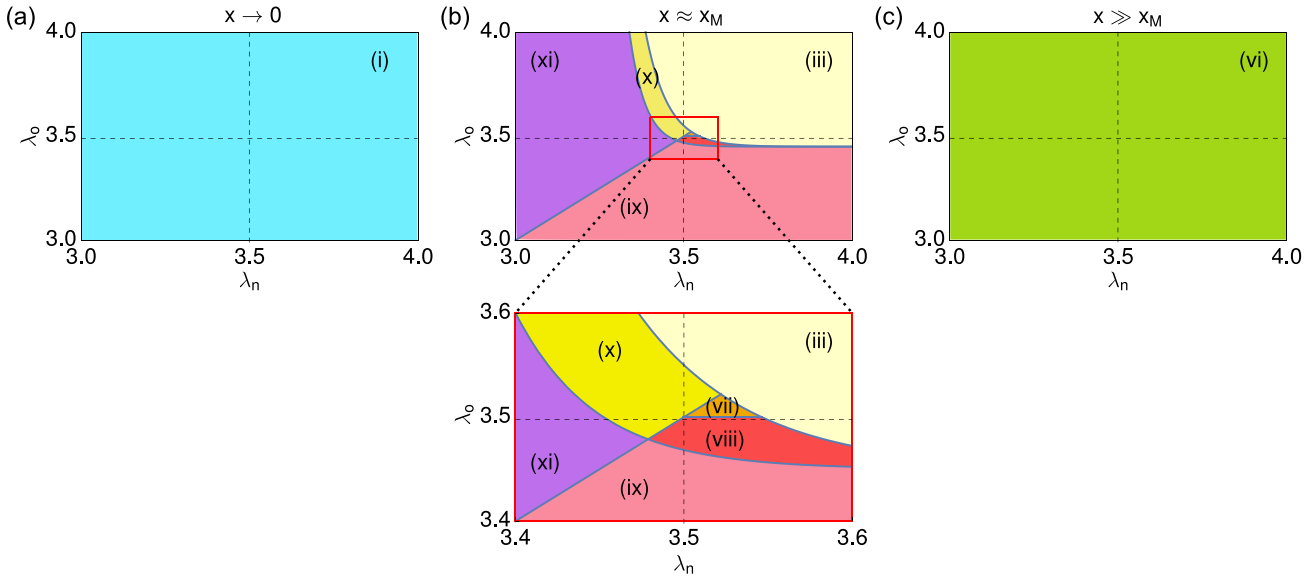


FIG. 6. Schematic phase diagrams of the  $g$ -AT model in the parameter space  $[\lambda_n, \lambda_o]$  for (a)  $x \approx 0$ , (b)  $x = x_M$ , and (c)  $x \gg x_M$ . The notations of the phases (i)–(vii) are the same as the ones presented in Figs. 3 and 10.

opinion spreads abruptly over a finite fraction of nodes in the multiplex network.

In region (vii)<sub>4</sub> ( $x'_e < x < x'_{g2}$ ), two continuous PTs occur successively: between the Para and the Coherent phase at  $T_{s,M}$  and between the Coherent and the Baxter phase at  $T'_s$ . Then as the temperature is decreased further two discontinuous jumps of the order parameter occur at  $T_f$  and  $T'_f$ , respectively. Overall, as the noise is reduced, the opinion dynamics exhibits two types of continuous PTs successively in which the coherent and the majority opinion are formed, respectively. When the noise is decreased further, the majority opinion spreads abruptly twice over a finite fraction of nodes in the multiplex network.

(2) In regions or points (viii) and (x) of Fig. 6 and Figs. 7(c) and 7(d), respectively, a continuous PT between the Para and the Baxter phase and a discontinuous jump of the order parameters  $m_a$  and  $M$  occur successively as the temperature is lowered. The critical behavior at  $x_M$  differs from that in region (ii) as we observe at a tricritical point. The transition point at  $x_M$  in (viii) and (x) acts as a branching point of the critical line to the two critical lines of the Coherent phase. Overall, as the noise is reduced the opinion dynamics exhibits first a continuous PT in which a majority opinion is formed in both layers, and subsequently the majority opinion spreads abruptly over a large fraction of nodes in the multiplex network.

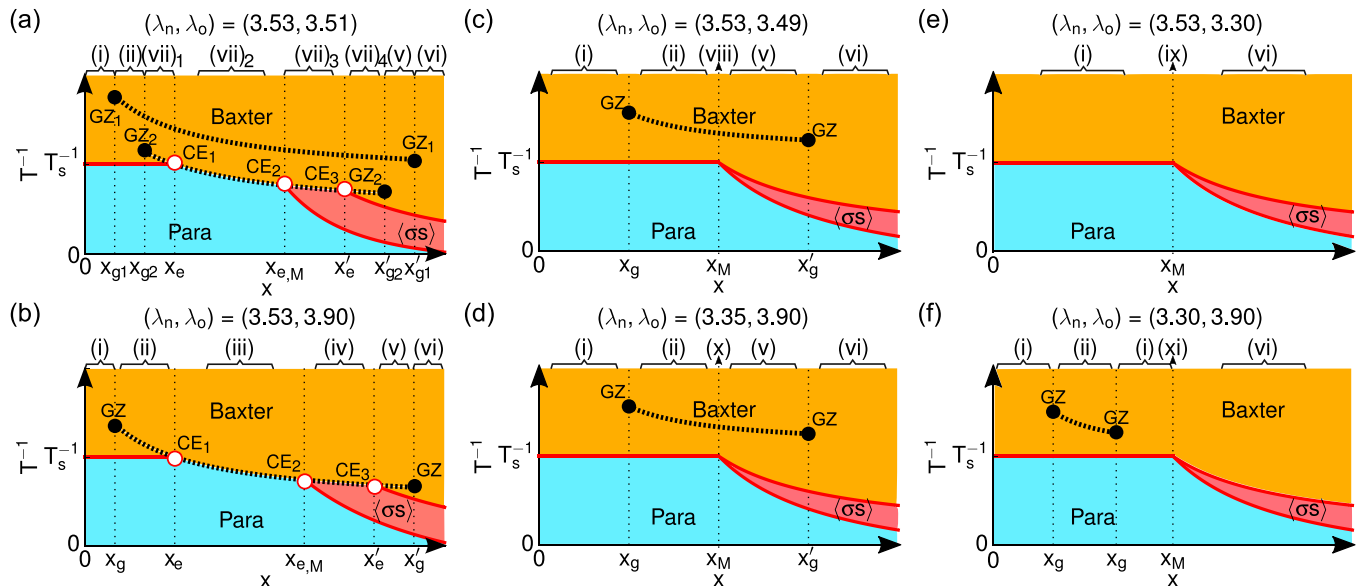


FIG. 7. Schematic phase diagrams of the  $g$ -AT model in the parameter space  $[x, T^{-1}]$  for various values  $\lambda_n$  and  $\lambda_o$ .  $(\lambda_n, \lambda_o) =$  (a) (3.53, 3.51), (b) (3.53, 3.90), (c) (3.53, 3.49), (d) (3.35, 3.90), (e) (3.53, 3.30), and (f) (3.30, 3.90).

(3) In regions (ix) and (xi) of Fig. 6 and in Figs. 7(e) and 7(f) at  $x_M$ , respectively, a continuous PT between the Para and the Baxter phase is observed as the temperature is lowered. The critical behavior at  $x_M$  differs from that in (i) as we observe at a tricritical point. The transition point at  $x_M$  in (ix) and (xi) acts as a branching point of the critical line to the two critical lines of the Coherent phase. As the noise is reduced, the opinion dynamics has continuous PT in which a majority opinion is formed in both layers.

To explore the dependence of this rich phase diagram on the exponents  $\lambda_n$  and  $\lambda_o$  around  $x = x_M$ , we plot the phase diagram in the space  $[x, T^{-1}]$  for various values of the degree pairs  $(\lambda_n, \lambda_o)$  (see Fig. 7). We find that if a first-order PT occurs at  $x = x_M$ , the overall phase diagram is close to the phase diagram discussed in Sec. IV [see Fig. 3 and Fig. 7(b)]. If  $x_M$  demarks the boundary between type-(ii) and type-(v) PTs, then the phase diagram is similar to Figs. 7(c) and 7(d), respectively. When  $\lambda_n < \lambda_o \approx 3.90$  [see Figs. 7(b), 7(d) and 7(f)], as  $\lambda_n$  is decreased, a discontinuous transition curve shrinks and moves left and upward as shown in Figs. 7(b)  $\rightarrow$  7(f). Moreover, when  $\lambda_n$  is slightly larger than  $\lambda_o \approx \lambda_c^+$  [see Fig. 7(a)], double discontinuous transition curves appear in the phase diagram, where two discontinuous PTs occur successively as  $T$  is decreased.

### C. Free-energy landscape for the $\lambda$ -dependence of phase transitions at $x \approx x_M$

Here, we will investigate the free-energy landscape of the  $g$ -AT model for the (vii)–(xi) types of PTs. Around  $x \approx x_M$ , phase and PT type are determined by the free-energy density presented in Appendix D.

In region (vii)<sub>1</sub>, PT type is determined by the free-energy density given as Eq. (D8) because  $x < x_M$ . Note that the higher-order term Eq. (D10) of Eq. (D8) is negative. As  $x \rightarrow x_M$ , the terms with  $B_o$  of Eq. (D10) and with  $D_m$  of Eq. (D8) become comparable in their magnitudes to the terms with  $C_3$  and  $D_o$  in Eq. (D24), respectively. Thus, these terms with  $D_m$  and  $B_o$  play a similar role to the terms with  $C_o$  and  $C_3$ . For  $T > T_s$ , the terms with  $D_m$  and  $B_o$  are not large in magnitude, so that the global minimum of  $f(m_a)$  remains at  $m_a = 0$  and  $M = 0$ , and thus a continuous PT occurs at  $T_s$ . However, when  $T$  is lowered further, the term with  $D_m$  increases and becomes comparable to the leading order terms. Then a discontinuous jump of the order parameters occurs at  $T_f$ . As  $T$  is lowered further, another negative term with  $B_o$  term increases, another jump of the order parameters occurs at  $T'_f$ . Hence in the region (vii)<sub>1</sub>, as  $T$  is lowered from  $T_s^+$ , a second-order PT occurs first, and then two discontinuous jumps occur successively in the Baxter phase.

In region (vii)<sub>2</sub>, the term with  $C_o$ , induced by the correlation between  $m_o$ s on different layers, becomes negative when  $\lambda_o > \lambda_c$ , thus produces a discontinuous PT at  $T_f$  higher than  $T_s$ . Another negative term with  $C_3$ , induced by the correlations between  $m_n$  of one layer and  $m_n$  or  $m_o$  of the other layer, becomes larger as  $T$  is decreased, and thus a discontinuous jump of the order parameters  $m_a$  and  $M$  in the Baxter phase occurs at  $T'_f < T_s$ .  $f(m_a)$  and  $f(M)$  develop a global minimum at a temperature  $T_f$ , leading to a discontinuous PT between the Para and the Baxter phase. As  $T$  is further lowered from  $T_f$ , the

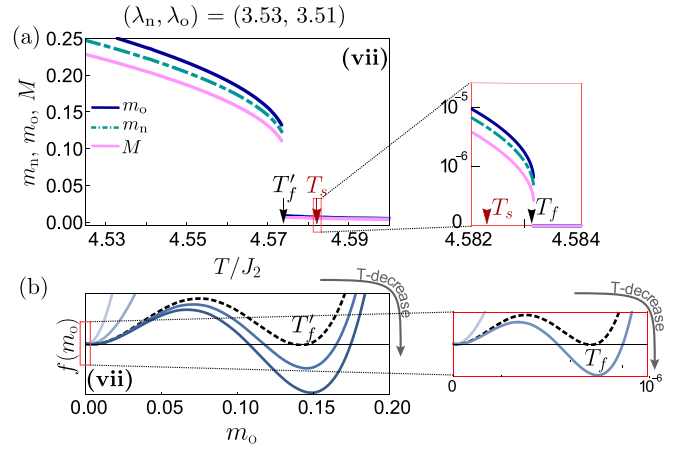


FIG. 8. For the (vii)-type of PT, schematic plots of (a) the order parameters  $m_a$  and  $M$  as a function of  $T$  and (b) the free-energy density landscape as a function of  $m_o$  for various  $T$ s. The exponents of degree distributions are taken as  $(\lambda_n, \lambda_o) = (3.53, 3.51)$ .

global minimum position of  $m_a$  and  $M$  increases continuously until a certain temperature  $T'_f$ . When  $T$  reaches  $T'_f$ , another global minimum of  $f(m_a)$  and  $f(M)$  emerge at another finite  $m_a$  and  $M$ , which lead to the jumps in the order parameters  $m_a$  and  $M$  in the Baxter phase. The order parameters and free energy landscape in this region are depicted in Figs. 8(a) and 8(b), respectively.

In region (vii)<sub>3</sub>, PT type is determined by the free-energy density Eq. (D19), because  $x > x_M$ . Note that the higher-order term Eq. (D21) of Eq. (D19) is negative. As  $x \rightarrow x_M$ , the terms with  $B'_o$  of Eq. (D21) and with  $D_M$  of Eq. (D19) become comparable in their magnitudes to the terms with  $C_3$  and  $D_o$  in Eq. (D24), respectively. Thus, these terms with  $D_M$  and  $B'_o$  play a similar role to the terms with  $C_o$  and  $C_3$ . For  $T > T_{s,M}$ , the terms with  $D_M$  and  $B'_o$  are small in magnitude, so that a global minimum of  $f(m_a)$  and  $f(M)$  remain at  $m_a = 0$  and  $M = 0$ , respectively. As  $T$  is lowered from  $T_{s,M}^+$ , a second-order PT for  $M$  occurs from the Para to the Coherent phase at  $T_{s,M}$  and a global minimum of  $f(M)$  increases continuously. When  $T$  is decreased further to  $T_f$ , the term with  $D_M$  increases in its magnitude, a new global minimum of  $f(m_a)$  and  $f(M)$  appears far from values at  $T_f^+$ , respectively, a discontinuous PT between the Coherent and the Baxter phase appears at  $T_f$ . When  $T$  is lowered further, the term with  $B'_o$  becomes large, a discontinuous jump of the order parameters occurs at  $T'_f$  in the Baxter phase. Hence, in the region (vii)<sub>3</sub>, as  $T$  is lowered from  $T_{s,M}^+$ , a continuous PT from the Para to the Coherent phase occurs first at  $T_{s,M}$ , and then a discontinuous PT between the Coherent and the Baxter phase occurs at  $T_f$  and then a discontinuous jump occurs at  $T'_f$  successively.

In region (vii)<sub>4</sub>, PT type is investigated through Eq. (D19), because  $x > x_M$ . When  $T > T_{s,M}$ , the terms with  $D_M$  and  $B'_o$  are too small, and the global minimum of  $f(m_a)$  and  $f(M)$  remain at  $m_a = 0$  and  $M = 0$ , respectively. For  $T'_s < T < T_{s,M}$ , a second-order PT for  $M$  from the Para to the Coherent phase occurs at  $T_{s,M}$ , and the global minimum of  $f(M)$  grows continuously as  $T$  is lowered from  $T_{s,M}^+$ . Meanwhile, the global minimum of  $f(m_a)$  remains at still  $m_a = 0$ . As  $T$  is lowered across  $T'_s$ , a second-order PT for  $m_a$  from the Coherent to the

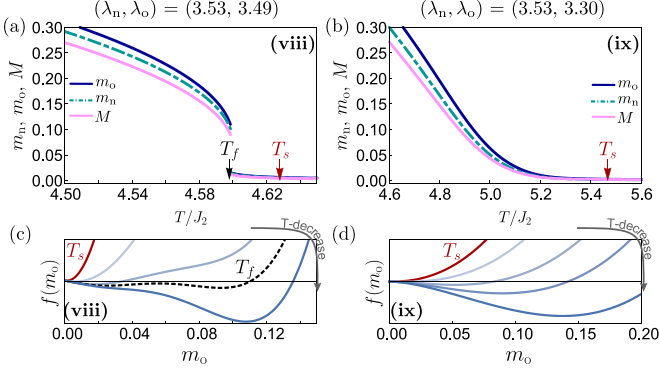


FIG. 9. For the (viii)- and (ix)-type of PTs, schematic plots of (a) and (b) the order parameters  $m_a$  and  $M$  as a function of  $T$ , respectively. (c) and (d) schematic plots of the free-energy density landscape as a function of  $m_a$  for the temperatures around  $T_f$ . The exponents of degree distributions for (a) and (c) are taken as  $(\lambda_n, \lambda_o) = (3.53, 3.30)$  and for (b) and (d) are taken as  $(3.53, 3.49)$ .

Baxter phase occurs at  $T'_s$ . When  $T$  is lowered and reaches  $T_f$  and  $T'_f (< T_f)$ , the global minimum of  $f(m_a)$  and  $f(M)$  jump discontinuously from the previous positions at  $T_f^+$  and  $T_f'^+$ , respectively. Hence, in the region (vii)<sub>4</sub>, as  $T$  is decreased from  $T_{s,M}^+$ , a continuous PT from the Para to the Coherent phase occurs at  $T_{s,M}$  and a continuous PT from the Coherent to the Baxter phase occurs at  $T'_s$ , and then two discontinuous jump of the order parameters in the Baxter phase occur at  $T_f$  and  $T'_f$ , successively.

In region (viii),  $f(m_a)$  and  $f(M)$  still display a global minimum at  $m = 0$  and  $M = 0$  for  $T > T_s$  and a continuous PT between the Para and the Baxter phase at  $T = T_s$ . The values of the critical exponents for this PT are listed in Table I for the case  $x \approx x_M$  and  $\lambda_n > \lambda_o$ . However, as  $T$  is further lowered below a certain temperature  $T_f$ , a global minimum emerges at a nonzero value of the magnetization  $m_a > 0$  and  $M > 0$ , and a discontinuous transition occurs. Thus, as  $T$  is decreased from  $T_s^+$ , a continuous transition occurs first at  $T_s$ , followed by a discontinuous transition at  $T_f$ . The order parameters and free-energy density landscape are depicted in Figs. 9(a) and 9(c), respectively.

In region (ix),  $f(m_a)$  and  $f(M)$  have a global minimum at  $m_a = 0$  and  $M = 0$ , respectively, for  $T \geq T_s$  while for  $T = T_s^-$  a global minimum emerges continuously at a nonzero value of the magnetization. Therefore, at  $T = T_s$  we observe a continuous PT between the Para and the Baxter phase. The values of the critical exponents for this PT are listed in Table I for the case  $x \approx x_M$  and  $\lambda_n > \lambda_o$ . The order parameters and free-energy density landscape are illustrated in Fig. 9(b) and 9(d), respectively. This continuous transitions is similar to the (i)-type PTs; however, the critical behavior for  $M$  of this continuous transition differs from that of the (i)-type PT, and thus we denote this type of a continuous transition as the (ix)-type PT to distinguish this from the (i)-type PTs.

In region (x),  $f(m_a)$  and  $f(M)$  have a global minimum at  $m_a = 0$  and  $M = 0$ , respectively.  $f(m_a)$  remains at  $m_a = M = 0$  for  $T > T_s$ . When  $T$  is lower than  $T_s$ , a continuous transition occurs. The values of the critical exponents for this PT are listed in Table I for the case  $x \approx x_M$  and  $\lambda_n < \lambda_o$ . As  $T$

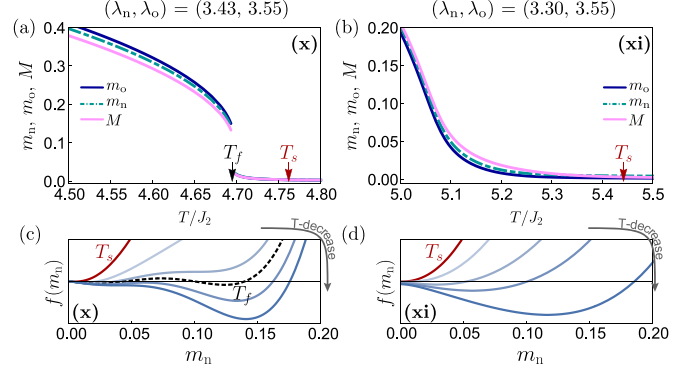


FIG. 10. (a), (b) Plots of the order parameters  $m_a$  and  $M$  at  $x = x_M$  as a function of  $T/J_2$ . (c), (d) Plots of the free-energy density landscape as a function of  $m_n$  for various  $T$ . The exponents of degree distributions taken for panels (a) and (c) are  $(\lambda_n, \lambda_o) = (3.30, 3.55)$  and for panels (b) and (d) are  $(3.43, 3.55)$ .

is further lowered, the order parameter gradually increases. When  $T$  reaches  $T_f$ , the order parameter jumps by a finite amount and a new global minimum of  $f(m_a)$  occurs at a finite  $m_a$ . Thus, as  $T$  is decreased from  $T_s^+$ , a continuous PT occurs at  $T_s$  first, and then a discontinuous jump of the order parameter occurs at  $T_f$  as shown in Figs. 10(a) and 10(b).

In region (xi),  $f(m_a)$  and  $f(M)$  have a global minimum at  $m_a = 0$  and  $M = 0$ , respectively. They remain at  $m_a = M = 0$  for  $T > T_s$ . At  $T_s$ ,  $m_a$  and  $M$  exhibit continuous PTs. The values of the critical exponents for this PT are listed in Table I for the case  $x \approx x_M$  and  $\lambda_n < \lambda_o$ . When  $T$  is decreased from  $T_s$ , a global minimum occurs at finite  $m_a$  and  $M$ . These behaviors are schematically shown in Figs. 10(b) and 10(d). Note that the  $\beta_M$  and  $\chi_M$  of the (xi)-type PTs are different from those of the (i)-type PTs [Eq. (30) and  $\gamma_M = 0$ ].

#### D. $\lambda$ -dependence of the Coherent phase

When  $x \rightarrow 0$ , a second-order PT occurs from the Baxter to the Para phase, whereas when  $x \gg x_M$ , a first-order PT occurs from the Baxter to the Coherent phase (i.e.,  $(\sigma s)$ ), followed by another PT occurs from the Coherent to the Para phase. The Coherent phase appears for  $x \geq x_{e,M}(\lambda_a)$ . In Fig. 11, we display the  $\lambda_a$ -dependence of  $x_{e,M}$  in unit of  $x_M$ . If  $x_{e,M} = x_M^+$ , then the Coherent phase appears in the range of  $x > x_M$  as shown in Figs. 7(a), 7(b) 7(d), and 7(e), which is denoted as (ix), (viii), (xi), and (x) (light yellow) in Fig. 11, respectively. In the regions (iii) and (vii), when a discontinuous PT occurs at  $x_M$ , then  $x_{e,M} > x_M$ , and the Coherent phase appears in range of  $x > x_{e,M}$  as shown in Figs. 7(c) and 7(f), respectively. The contour lines between different regions with different circle numbers represent different ratios  $x_{e,M}/x_M$ .

We find that the transition point  $x_{e,M}$  is delayed as both  $\lambda_n$  and  $\lambda_o$  are increased. This is caused by the following reasons: if  $\lambda_n$  and  $\lambda_o$  are large, then the branching ratios of nonoverlapping and overlapping links, respectively, become small. Thus, a larger value of  $x = J_4/J_2$  is needed, i.e., the strength of four-body interaction needs to be reinforced to form a Coherence phase.



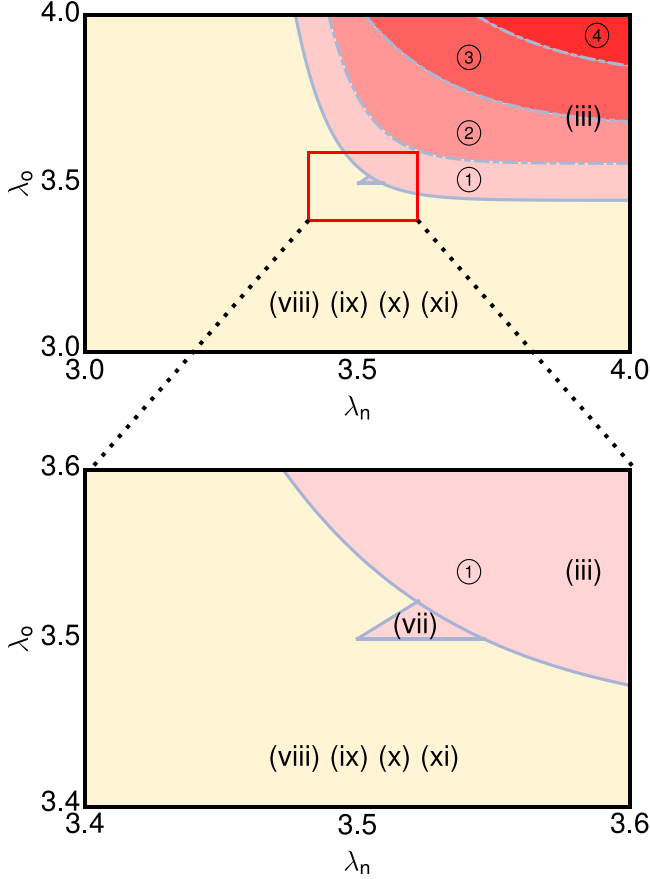


FIG. 11. Schematic contour lines of  $x_{e,M}$  in the parameter space  $[\lambda_n, \lambda_o]$ . The rightmost (light yellow) region contains the domains (viii), (ix), (x), and (xi) as shown in Fig. 6(b). In this region, a continuous PT appears at  $T_s$  at  $x_M$ , and thus  $x_{e,M} = x_M$ , the Coherent phase appears at  $x_M$ . The regions denoted as ① – ④ correspond to the regions (iii) and (vii) denoted in Fig. 6(b). In this region, a discontinuous PT appears at  $x_M$ , and thus  $x_{e,M} > x_M$ . The contour lines represent in term of the ratio  $x_{e,M}/x_M$ . In ①,  $1 < x_{e,M}/x_M < 1.05$ ; in ②,  $1.05 < x_{e,M}/x_M < 1.10$ ; in ③,  $1.10 < x_{e,M}/x_M < 1.15$ ; and in ④,  $1.15 < x_{e,M}/x_M$ .

## VI. CONCLUSION

To investigate the effect of link overlap on the opinion dynamics defined on a multiplex network, we studied the so-called  $g$ -AT model, a spin model in thermal equilibrium systems. The  $g$ -AT model describes the dynamics of two species of Ising spins, namely, the  $s$  and  $\sigma$  spins, each of which is located on a single layer of the duplex network under consideration. Here, the spin model is defined on duplex networks with an SF multidegree distribution, which facilitates tuning of the effect of overlapping links with respect to nonoverlapping links. In particular, we distinguish between multilinks (1,1) that characterize overlapping links and multilinks (1,0) and (0,1) that do not. We assume that the multidegrees  $k^{(1,1)} = k_o$  and  $k^{(1,0)} = k^{(0,1)} = k_n$  follow power-law distributions associated with the tunable power-law exponents  $\lambda_n$  and  $\lambda_o$ . This system is illustrated in Fig. 1.

Pairs of  $s$ -spins (pairs of  $\sigma$ -spins) connected by overlapping and nonoverlapping links interact through a 2-body interaction of strength  $J_2$ . Four spins comprising two  $s$ -spins and two  $\sigma$ -spins connected by overlapping links interact through a four-body interaction with strength  $J_4$  (see Fig. 2). The ratio  $x \equiv J_4/J_2$  is a control parameter that can alter the critical properties of the model, and the system is assumed to be in thermal contact with a heat reservoir at temperature  $T$ . Here,  $T$  represents the diversity of each individual opinion in a social community. Thus, there exist four control parameters, namely,  $\lambda_n$ ,  $\lambda_o$ ,  $x$ , and  $T$ . By applying the Landau–Ginzburg theory, we obtained rich phase diagrams in the four-parameter space. The  $g$ -AT model is a generalization of the original AT model [40], in which all the links are regarded as overlapping links; therefore, a single exponent  $\lambda_o$  is considered in this context.

We note that the different species of spins represent individuals from two different communities formed based on friendship and business relations, respectively. Each pair of individuals may be connected solely via friendship links, solely via business relations, or via both relationships. The formation of a majority opinion across both layer is indicated by the magnetizations  $\langle \sigma \rangle > 0$ ,  $\langle s \rangle > 0$ , and  $\langle \sigma s \rangle > 0$  in the spin model, which can be accomplished through nonoverlapping or overlapping links. The diversity of individual opinions is reflected by thermal fluctuations.

We investigated PTs arising from the competition between the consensus formation of each community and that of the entire society, and obtained rich phase diagrams including diverse types of PTs. These findings are expected to be beneficial in understanding the underlying mechanisms of local and global formation of a majority opinion in a society.

Similar to the voter models on multiplex networks [35], the  $g$ -AT model shows that a majority opinion emerges abruptly thanks to the interactions across two layers induced by overlapping links. In particular, in the  $g$ -AT model, we can control the strength of four-body interactions among replica nodes connected by overlapping multilinks with respect of the strength of two-body interactions  $x = J_4/J_2$ . This allows us to assess the role of tuning the strength of the many-body AT-interactions by modulating  $x$  and study how the phase diagram change with respect to the original AT model [40]. Moreover, we can tune the power-law exponent of the overlapping multidegree distributions of nonoverlapping and overlapping multilinks  $(\lambda_n, \lambda_o)$ , and investigate the role of this topological modifications on PTs, in the same spirit of the analysis conducted for percolation problems in Refs. [21,24]. In the future our work can be expanded in many directions, investigating further the role that higher-order interactions [45,46] have in opinion dynamics defined on multiplex networks and exploring realistic spin models of opinion dynamics defined on duplex networks.

## ACKNOWLEDGMENTS

This research was supported by NRF Grant No. NRF-2014R1A3A2069005, KENTECH Research Grant No. KRG2021-01-007 (B.K.), and KIAS individual Grant No. PG064901 (J.S.L.) at Korea Institute for Advanced Study.

**APPENDIX A: SELF-CONSISTENCY EQUATION WITH AN EXTERNAL MAGNETIC FIELD**

With the external magnetic field,

$$\Omega_a \equiv K_2 m_a + H_a \quad \text{and} \quad \Omega_M \equiv K_4 M + H_4, \quad (\text{A1})$$

the self-consistency equations Eqs. (24) for  $m_a$  and  $M$  of the  $g$ -AT model are replaced as follows:

$$m_a \langle k_a \rangle = m_{aI} \equiv \int_{k_{\min}^n}^{\infty} \int_{k_{\min}^o}^{\infty} dk_n dk_o P_d(k_n) P_d(k_o) \frac{\tanh(\Omega_o k_o + \Omega_n k_n) [1 + \tanh(\Omega_4 k_o)]}{1 + \tanh^2(\Omega_o k_o + \Omega_n k_n) \tanh(\Omega_4 k_o)} k_a \quad (\text{A2})$$

and

$$M \langle k_o \rangle = M_I \equiv \int_{k_{\min}^n}^{\infty} \int_{k_{\min}^o}^{\infty} dk_n dk_o P_d(k_n) P_d(k_o) \frac{\tanh(\Omega_4 k_o) + \tanh^2(\Omega_o k_o + \Omega_n k_n)}{1 + \tanh^2(\Omega_o k_o + \Omega_n k_n) \tanh(\Omega_4 k_o)} k_o. \quad (\text{A3})$$

**APPENDIX B: DEFINITIONS OF THE  $\mathcal{A}$  TERMS IN EXACT SUSCEPTIBILITY FORMULA**

The  $\mathcal{A}$  terms are defined as follows:

$$\mathcal{A}_{aa} = \int_{k_{\min}^n}^{\infty} \int_{k_{\min}^o}^{\infty} dk_n dk_o P_d(k_n) P_d(k_o) \frac{(1 - \mathcal{T}_2^2 \mathcal{T}_4)(1 + \mathcal{T}_4)}{(1 + \mathcal{T}_2^2 \mathcal{T}_4)^2 \cosh^2(K_2(m_o k_o + m_n k_n))} k_a^2, \quad (\text{B1})$$

$$\mathcal{A}_{a\bar{a}} = \mathcal{A}_{\bar{a}a} = \int_{k_{\min}^n}^{\infty} \int_{k_{\min}^o}^{\infty} dk_n dk_o P_d(k_n) P_d(k_o) \frac{(1 - \mathcal{T}_2^2 \mathcal{T}_4)(1 + \mathcal{T}_4)}{(1 + \mathcal{T}_2^2 \mathcal{T}_4)^2 \cosh^2(K_2(m_o k_o + m_n k_n))} k_n k_o, \quad (\text{B2})$$

$$\mathcal{A}_{aM} = \int_{k_{\min}^n}^{\infty} \int_{k_{\min}^o}^{\infty} dk_n dk_o P_d(k_n) P_d(k_o) \frac{(1 - \mathcal{T}_2^2) \mathcal{T}_4}{(1 + \mathcal{T}_2^2 \mathcal{T}_4)^2 \cosh^2(K_4 M k_o)} k_a k_o, \quad (\text{B3})$$

$$\mathcal{A}_{Ma} = \int_{k_{\min}^n}^{\infty} \int_{k_{\min}^o}^{\infty} dk_n dk_o P_d(k_n) P_d(k_o) \frac{2\mathcal{T}_2(1 - \mathcal{T}_4^2)}{(1 + \mathcal{T}_2^2 \mathcal{T}_4)^2 \cosh^2(K_2(m_o k_o + m_n k_n))} k_o k_a, \quad (\text{B4})$$

$$\mathcal{A}_{MM} = \int_{k_{\min}^n}^{\infty} \int_{k_{\min}^o}^{\infty} dk_n dk_o P_d(k_n) P_d(k_o) \frac{1 - \mathcal{T}_2^4}{(1 + \mathcal{T}_2^2 \mathcal{T}_4)^2 \cosh^2(K_4 M k_o)} k_o^2. \quad (\text{B5})$$

**APPENDIX C: DEFINITIONS OF COEFFICIENTS IN THE FREE-ENERGY DENSITY**

The coefficients  $C_o$ ,  $C_n$ ,  $D_m$ ,  $D_M$ ,  $D_0$ , and  $C_o(r_0, \lambda_o)$  used in the Landau free energy formulas in Appendix D are defined as follows:

$$C_o(\lambda_o) = C_M(\lambda_o) = -N_o \int_0^{\infty} \left[ \ln(\cosh y) - \frac{1}{2} y^2 \right] y^{-\lambda_o} dy,$$

$$C_n(\lambda_n) = -N_n \int_0^{\infty} \left[ \ln(\cosh y) - \frac{1}{2} y^2 \right] y^{-\lambda_n} dy,$$

$$D_m(\lambda_o) = -N_o \int_0^{\infty} y \ln(1 + \tanh^2 y) y^{-\lambda_o} dy,$$

$$D_M(\lambda_o) = -N_o \int_0^{\infty} y^2 \ln(1 + \tanh y) y^{-\lambda_o} dy,$$

$$D_0(r_0, \lambda_o) = -N_o \int_0^{\infty} \ln[1 + \tanh^2 y \tanh(r_0 y)] y^{-\lambda_o} dy,$$

$$C_o(r_0, \lambda_o) = C_o(\lambda_o) + D_0(r_0, \lambda_o) + \frac{1}{2} C_M(\lambda_o), \quad (\text{C1})$$

where  $N_o$  and  $N_n$  are normalization factors written as  $1/(\lambda_o - 1)$  and  $1/(\lambda_n - 1)$ , respectively.

**APPENDIX D: LANDAU FREE ENERGY FORMULA**

To investigate the critical behavior near the critical temperature, we expand the free-energy density as a function of the order parameters  $m_a$  and then analyze the leading terms when  $m_a$  and  $M$  converge to 0. To proceed, it is necessary to derive the relation between  $m_a$  and  $M$ , which turns out to depend on the ratio  $x$ . For values of  $x$  smaller and bigger than the characteristic ratio  $x_M$ , we observe different behaviors. Here we discuss in details the cases  $0 < x < x_M$ ,  $x > x_M$ , and  $x = x_M$ , separately.

### 1. Case $0 < x < x_M$

For  $x \in (0, x_M)$  we can expand Eqs. (21) and (22) in terms of  $m_a$  and  $M$  within the lowest-order terms as follows:

$$m_n \langle k_n \rangle \left( 1 - K_2 \frac{\langle k_n^2 \rangle}{\langle k_n \rangle} \right) \simeq K_2 m_o \langle k_n \rangle \langle k_o \rangle - (\lambda_n - 1) C_n(\lambda_n) (K_2 m_n)^{\lambda_n - 2} + \text{h.o.}, \quad (\text{D1})$$

$$m_o \langle k_o \rangle \left( 1 - K_2 \frac{\langle k_o^2 \rangle}{\langle k_o \rangle} \right) \simeq K_2 m_n \langle k_n \rangle \langle k_o \rangle - (\lambda_o - 1) C_o(\lambda_o) (K_2 m_o)^{\lambda_o - 2} + (\lambda_o - 2) D_m(\lambda_o) (K_4 M) (K_2 m_o)^{\lambda_o - 3} + \text{h.o.}, \quad (\text{D2})$$

$$M \langle k_o \rangle \left( 1 - x K_2 \frac{\langle k_o^2 \rangle}{\langle k_o \rangle} \right) \simeq D_m(\lambda_o) (K_2 m_o)^{\lambda_o - 2} - (\lambda_o - 1) C_M(\lambda_o) (K_4 M)^{\lambda_o - 2} + \text{h.o.}, \quad (\text{D3})$$

where the coefficients of the entropy terms  $C_a(\lambda_a)$  and  $C_M(\lambda_o)$  are presented in Appendix C and the coefficient of the interlayer interaction term  $D_m(\lambda_o)$  of the right-hand side of Eq. (D2) is also presented in Appendix C. This term needs to be considered, because it is negative and contributes to the first-order transition.

To obtain  $T_s$ , we first consider the lowest-order terms of Eqs. (D1) and (D2) and obtain the following:

$$\left( 1 - \frac{\langle k_o^2 \rangle}{\langle k_o \rangle} \frac{1}{T} \right) \left( 1 - \frac{\langle k_n^2 \rangle}{\langle k_n \rangle} \frac{1}{T} \right) - \frac{1}{T^2} \langle k_n \rangle \langle k_o \rangle = 0. \quad (\text{D4})$$

This equation has two solutions of  $T$ , denoted as  $T_\ell$  and  $T_h$ .

It is guaranteed that the left-hand side of Eq. (D3) is positive as  $T \rightarrow T_h^-$  as long as  $x < x_M$  with

$$x_M \equiv T_h \langle k_o \rangle / \langle k_o^2 \rangle. \quad (\text{D5})$$

Then  $M$  is written within a leading order as

$$M \simeq \frac{D_m(\lambda_o)}{\langle k_o \rangle [1 - x T_h / (x_M T)]} (K_2 m_o)^{\lambda_o - 2} + \text{h.o.} \quad (\text{D6})$$

This implies that  $O(M) \ll O(m_a)$  near  $T_h^-$  for  $\lambda_o > 3$ . Using this relation Eq. (D6), we obtain the self-consistency relations for  $m_a$  with leading terms as follows:

$$m_a \langle k_n \rangle \langle k_o \rangle \left( 1 - \frac{T_\ell}{T} \right) \left( 1 - \frac{T_h}{T} \right) \simeq -(\lambda_a - 1) E_{\bar{a}} C_a(\lambda_a) (K_2 m_a)^{\lambda_a - 2} - (\lambda_{\bar{a}} - 1) F_{\bar{a}\bar{a}} C_{\bar{a}}(\lambda_{\bar{a}}) (K_2 m_{\bar{a}})^{\lambda_{\bar{a}} - 2}, \quad (\text{D7})$$

where  $E_{\bar{a}} = \langle k_{\bar{a}} \rangle (1 - \frac{\langle k_{\bar{a}}^2 \rangle}{\langle k_{\bar{a}} \rangle})$  and  $F_{\bar{a}\bar{a}} = \frac{1}{T} \langle k_n \rangle \langle k_o \rangle$ .

As  $T \rightarrow T_h^-$ ,  $m_a \rightarrow 0$  and thus  $M \rightarrow 0$  in Eq. (D6). This implies that the PT from Baxter to Para phase is continuous. We confirm that a second-order transition occurs at  $T_h$ . This temperature is denoted as a critical temperature  $T_s \equiv T_h$ .

Using Eq. (D6), we expand the free-energy density of Eq. (18) with respect to  $m_a$  up to the three lowest order terms:

(i) For  $\lambda_n > \lambda_o$ ,

$$f(m_o) \simeq A_o K_2 m_o^2 \left( 1 - \frac{T_s}{T} \right) + C_o(\lambda_o) (K_2 m_o)^{\lambda_o - 1} + C_n(\lambda_n) (B_o m_o)^{\lambda_n - 1} - \frac{1}{2} \frac{K_4 [D_m(\lambda_o)]^2}{\langle k_o \rangle [1 - x T_s / (x_M T)]} (K_2 m_o)^{2(\lambda_o - 2)} + \text{h.o.}, \quad (\text{D8})$$

where  $A_o$  and  $B_o$  are functions of  $\lambda_a$  and  $K_2$ , for which the explicit formula is as follows:

$$A_o(\lambda_o) = \frac{K_2 \langle k_n \rangle^2 K_2 \langle k_o \rangle^2}{\langle k_n \rangle - K_2 \langle k_n^2 \rangle}, \quad B_o(\lambda_o) = \frac{K_2 \langle k_n \rangle K_2 \langle k_o \rangle}{\langle k_n \rangle - K_2 \langle k_n^2 \rangle}. \quad (\text{D9})$$

There is an additional negative higher-order term as follows:

$$\frac{D_m(\lambda_o)}{\langle k_o \rangle [1 - x T_h / (x_M T)]} (K_2 m_o)^{\lambda_o} \left[ \frac{\lambda_o - 1}{\lambda_o - 3} (k_{\min}^o)^{3 - \lambda_o} + 2 \frac{B_o}{K_2} \langle (k^n) \rangle \langle (k^o)^2 \rangle + \left( \frac{B_o}{K_2} \right)^2 \langle (k^n)^2 \rangle \langle (k^o) \rangle \right]. \quad (\text{D10})$$

Note that as  $x \rightarrow x_M^-$ , the magnitude of Eq. (D10) becomes comparable to that of the term with  $C_3$ .

(ii) For  $\lambda_n < \lambda_o$ ,

$$f(m_n) \simeq A_n K_2 m_n^2 \left( 1 - \frac{T_s}{T} \right) + C_n(\lambda_n) (K_2 m_n)^{\lambda_n - 1} + C_o(\lambda_o) (B_n m_n)^{\lambda_o - 1} - \frac{1}{2} \frac{K_4 [D_m(\lambda_o)]^2}{\langle k_o \rangle [1 - x T_s / (x_M T)]} (B_n m_n)^{2(\lambda_o - 2)} + \text{h.o.}, \quad (\text{D11})$$

where  $A_n$  and  $B_n$  are functions of  $\lambda_a$  and  $K_2$ , for which the explicit formula is as follows:

$$A_n(\lambda_n) = \frac{K_2 \langle k_n \rangle^2 K_2 \langle k_o \rangle^2}{\langle k_o \rangle - K_2 \langle k_o^2 \rangle}, \quad B_n(\lambda_n) = \frac{K_2 \langle k_n \rangle K_2 \langle k_o \rangle}{\langle k_o \rangle - K_2 \langle k_o^2 \rangle}. \quad (\text{D12})$$

Note that  $C_a(\lambda_a)$  and  $D_m(\lambda_o)$  are always positive.

The phase diagram in the space of  $[x, T^{-1}]$  depends on  $\lambda_n$  and  $\lambda_o$  as shown in Fig. 4. These phase diagrams reveal the nature of the observed PTs and can be obtained by examining the profiles of the free-energy density for different  $x$  and  $T$  values for given  $\lambda_n$  and  $\lambda_o$ . To be concrete, here we consider the case of  $\lambda_n = 3.53$  and  $\lambda_o = 3.90$ , for which we obtain the phase diagram similar to that of the original AT model with the exponent of degree distribution  $\lambda > \lambda_c$ .

## 2. Case $x > x_M$

The self-consistency relations Eqs. (21) and (22) are expanded in terms of  $m_a$  and  $M$  as follows:

$$m_n \langle k_n \rangle \left( 1 - K_2 \frac{\langle k_n^2 \rangle}{\langle k_n \rangle} \right) \simeq K_2 m_o \langle k_n \rangle \langle k_o \rangle - (\lambda_n - 1) C_n(\lambda_n) (K_2 m_n)^{\lambda_n - 2} + (K_4 M) (K_2 m_n) \langle k_n^2 \rangle \langle k_o \rangle + (K_4 M) (K_2 m_o) \langle k_n \rangle \langle k_o^2 \rangle + \text{h.o.} \quad (\text{D13})$$

$$\begin{aligned} m_o \langle k_o \rangle \left( 1 - K_2 \frac{\langle k_o^2 \rangle}{\langle k_o \rangle} \right) &\simeq K_2 m_n \langle k_n \rangle \langle k_o \rangle - (\lambda_o - 1) C_o(\lambda_o) (K_2 m_o)^{\lambda_o - 2} \\ &+ D_M(\lambda_o) (K_4 M)^{\lambda_o - 3} (K_2 m_o) \\ &- \left[ \int_0^1 dk_o P_d(k_o) \tanh(K_4 M k_o) k_o^2 \right] (K_2 m_o) + (K_4 M) (K_2 m_n) \langle k_n \rangle \langle k_o^2 \rangle + \text{h.o.} \end{aligned} \quad (\text{D14})$$

$$M \langle k_o \rangle \left( 1 - x K_2 \frac{\langle k_o^2 \rangle}{\langle k_o \rangle} \right) \simeq -(\lambda_o - 1) C_M(\lambda_o) (K_4 M)^{\lambda_o - 2} + (\lambda_o - 3) D_M(\lambda_o) (K_4 M)^{\lambda_o - 4} (K_2 m_o)^2 + \text{h.o.}, \quad (\text{D15})$$

where  $D_M(\lambda_o) > 0$  increases monotonically with  $\lambda_o$ . This coefficient is explicitly derived in Appendix C. These expansions are valid for  $3 < (\lambda_n, \lambda_o) < 4$  due to the power of the third term of the right-hand side of Eq. (D14).

When  $x > x_M$ ,  $x \langle k_o^2 \rangle / \langle k_o \rangle > T_h$  and the left-hand side of Eq. (D15) becomes negative for  $T > T_h$ . However, the first term of the right-hand side of Eq. (D15) is also negative; however, the second term is positive. So, the first term is comparable to the left-hand side, leading to  $M \sim (T_{s,M}/T - 1)^{1/(\lambda_o - 3)}$ , where  $T_{s,M} \equiv x \langle k_o^2 \rangle / \langle k_o \rangle$ . Thus,  $M$  exhibits a continuous transition at  $T_{s,M}$ , corresponding to the continuous transition curve starting from CE<sub>2</sub> in Fig. 3. Note that this formula is the same as the one of the Ising model on a single SF network [2]. For further discussions,  $M_*$  is defined as

$$M_* \equiv \frac{1}{K_4} \left[ \frac{\langle k_o \rangle (T_{s,M}/T - 1)}{(\lambda_o - 1) K_4 C_M(\lambda_o)} \right]^{1/(\lambda_o - 3)}.$$

Next, to determine a critical temperature (denoted as  $T_{s,m}$ ) for  $m_a$ , we first rewrite Eq. (D15) as

$$M \simeq M_* + \frac{D_M(\lambda_o)}{\langle k_o \rangle (T_{s,M}/T - 1)} (K_4 M_*)^{\lambda_o - 4} (K_2 m_o)^2 + \text{h.o.} \quad (\text{D16})$$

We consider the linear terms of  $m_a$  in Eqs. (D13) and (D14), and substitute  $M$  with  $M_*$ . Using a similar technique used in Eq. (D4), we obtain the following:

$$\langle k_n \rangle \langle k_o \rangle \left( 1 - \frac{\langle k_n^2 \rangle / \langle k_n \rangle + g_n(M_*)}{T} \right) \left( 1 - \frac{\langle k_o^2 \rangle / \langle k_o \rangle + g_o(M_*)}{T} \right) - \left( \frac{\langle k_n \rangle \langle k_o \rangle}{T} + \frac{K_4 M_* \langle k_n \rangle \langle k_o^2 \rangle}{T} \right)^2 = 0, \quad (\text{D17})$$

where

$$g_n(M_*) \langle k_n \rangle = K_4 M_* \langle k_o \rangle \langle k_n^2 \rangle, \quad \text{and} \quad g_o(M_*) \langle k_o \rangle = D_M(\lambda_o) (K_4 M_*)^{\lambda_o - 3} - \int_0^1 dk_o P_d(k_o) \tanh(K_4 M_* k_o) k_o^2.$$

Equation (D17) has two solutions for  $T$ , denoted as  $T'_\ell$  and  $T'_h$  ( $T'_\ell < T'_h$ ). Using the relation Eq. (D16), we can obtain a self-consistency relation for  $m_a$  within the leading order as follows:

$$m_a \langle k_o \rangle \langle k_n \rangle \left( 1 - \frac{T'_\ell}{T} \right) \left( 1 - \frac{T'_h}{T} \right) \simeq -(\lambda_a - 1) E'_a C_a(\lambda_a) (K_2 m_a)^{\lambda_a - 2} - (\lambda_{\bar{a}} - 1) F'_{\bar{a}\bar{a}} C_{\bar{a}}(\lambda_{\bar{a}}) (K_2 m_{\bar{a}})^{\lambda_{\bar{a}} - 2}, \quad (\text{D18})$$

where  $E'_a = \langle k_{\bar{a}} \rangle (1 - \frac{\langle k_{\bar{a}}^2 \rangle / \langle k_{\bar{a}} \rangle + g_{\bar{a}}(M_*)}{T})$  and  $F'_{\bar{a}\bar{a}} = \frac{1}{T} \langle k_o \rangle \langle k_n \rangle + \frac{1}{T} K_4 M_* \langle k_o^2 \rangle \langle k_n \rangle$ . We find that near  $T'_h$ ,  $m_a$  converges to zero continuously, whereas  $M$  remains in  $O(1)$ . Hence, we regard  $T'_h$  as the critical temperature  $T'_s$  of  $m_a$ . Note that  $M$  has the critical temperature  $T_{s,M}$  separately, given as  $x \langle k_o^2 \rangle / \langle k_o \rangle$ , which is higher than  $T'_s$ .



Using Eq. (D16), we expand the free-energy density of Eq. (18) with respect to  $m_a$  up to the three lowest order terms:

(i) For  $\lambda_n > \lambda_o$ ,

$$f(m_o) \simeq f_0(M_*) + A'_o K_2 m_o^2 \left(1 - \frac{T'_s}{T}\right) + C_o(\lambda_o)(K_2 m_o)^{\lambda_o-1} + C_n(\lambda_n)(B'_o m_o)^{\lambda_n-1} \\ - \frac{K_2[(\lambda_n - 1)C_n(\lambda_n)]^2}{\langle k_n \rangle [1 - ((k_n^2)/\langle k_n \rangle + g_n(M_*))/T]} (B'_o m_o)^{2(\lambda_n-2)} - \frac{1}{2}(\lambda_o - 3) \frac{K_4 [D_M(\lambda_o)(K_4 M_*)^{\lambda_o-4}]^2}{\langle k_o \rangle (T_{s,M}/T - 1)} (K_2 m_o)^4 + \text{h.o.}, \quad (\text{D19})$$

where  $A'_o$  and  $B'_o$  are functions of  $\lambda_a$ ,  $K_2$  and  $K_4 M_*$ . They are explicitly derived as follows:

$$A'_o(\lambda_o) = \frac{(1 + K_4 M_* \langle k_o^2 \rangle / \langle k_o \rangle)^2 K_2 \langle k_n \rangle^2 K_2 \langle k_o \rangle^2}{\langle k_n \rangle [1 - K_2 ((k_n^2)/\langle k_n \rangle + g_n(M_*))]}, \quad B'_o(\lambda_o) = \frac{(1 + K_4 M_* \langle k_o^2 \rangle / \langle k_o \rangle) K_2 \langle k_n \rangle K_2 \langle k_o \rangle}{\langle k_n \rangle [1 - K_2 ((k_n^2)/\langle k_n \rangle + g_n(M_*))]}. \quad (\text{D20})$$

There is an additional negative higher-order term as follows:

$$\frac{D_M(\lambda_o)}{\langle k_o \rangle (T_{s,M}/T - 1)} (K_4 M_*)^{\lambda_o-4} (K_2 m_o)^4 \left[ \frac{\lambda_o - 1}{\lambda_o - 3} (k_{\min}^o)^{3-\lambda_o} + 2 \frac{B'_o}{K_2} \langle (k^n) \rangle \langle (k^o)^2 \rangle + \left( \frac{B'_o}{K_2} \right)^2 \langle (k^n)^2 \rangle \langle (k^o) \rangle \right]. \quad (\text{D21})$$

Note that as  $x \rightarrow x_M^+$ , Eq. (D10) becomes close in its magnitude to the term with  $C_3$  and thus, play a similar role to the term with  $C_3$  near  $x_M^+$ .

(ii) For  $\lambda_n < \lambda_o$ ,

$$f(m_n) \simeq f_0(M_*) + A'_n K_2 m_n^2 \left(1 - \frac{T'_s}{T}\right) + C_n(\lambda_n)(K_2 m_n)^{\lambda_n-1} + C_o(\lambda_o)(B'_n m_n)^{\lambda_o-1} \\ - \frac{K_2[(\lambda_o - 1)C_o(\lambda_o)]^2}{\langle k_o \rangle [1 - ((k_o^2)/\langle k_o \rangle + g_o(M_*))/T]} (B'_n m_n)^{2(\lambda_o-2)} - \frac{1}{2}(\lambda_o - 3) \frac{K_4 [D_M(\lambda_o)(K_4 M_*)^{\lambda_o-4}]^2}{\langle k_o \rangle (T_{s,M}/T - 1)} (B'_n m_n)^4 + \text{h.o.}, \quad (\text{D22})$$

where  $A'_n$  and  $B'_n$  are functions of  $\lambda_a$ ,  $K_2$  and  $K_4 M_*$ . They are explicitly derived as follows:

$$A'_n(\lambda_o) = \frac{(1 + K_4 M_* \langle k_o^2 \rangle / \langle k_o \rangle)^2 K_2 \langle k_n \rangle^2 K_2 \langle k_o \rangle^2}{\langle k_o \rangle [1 - K_2 ((k_o^2)/\langle k_o \rangle + g_o(M_*))]}, \quad B'_n(\lambda_o) = \frac{(1 + K_4 M_* \langle k_o^2 \rangle / \langle k_o \rangle) K_2 \langle k_n \rangle K_2 \langle k_o \rangle}{\langle k_o \rangle [1 - K_2 ((k_o^2)/\langle k_o \rangle + g_o(M_*))]}. \quad (\text{D23})$$

Here, first two  $C_a$  terms are positive, like the case  $x < x_M$ .

The first two  $C_a$  terms in Eqs. (D19) and (D22) are positive, as for the case  $x < x_M$ , whereas the next two terms containing  $C_a$  and  $D_M$  are negative. The  $2(\lambda_a - 2)$ -order terms with  $C_a$  are finite, whereas the  $D_M$  term diverges as  $T \rightarrow T_{s,M}$ . Thus, the  $D_M$  term contributes to the formation of a global minimum of  $f(m_a)$  as  $T$  is decreased  $T_f$  and  $x \rightarrow x_M^+$ .

### 3. Case $x \approx x_M$

#### a. Case $\lambda_n \geq \lambda_o$

In this case,  $O(m_a) \sim O(M)$  near  $T_s$  and the free-energy density of Eq. (18) is expanded with respect to  $m_o$  as follows:

$$f(m_o) \simeq A_o K_2 m_o^2 \left(1 - \frac{T'_s}{T}\right) + \frac{1}{2} K_4 M^2 \langle k_o \rangle \left(1 - \frac{T'_s}{T}\right) + C_o(\lambda_o, r_o)(K_2 m_o)^{\lambda_o-1} + C_n(\lambda_n)(B_o m_o)^{\lambda_n-1} + C_3(\lambda_n, \lambda_o, r_o)(K_2 m_o)^3 + \text{h.o.}, \quad (\text{D24})$$

where  $A_o$  and  $B_o$  are functions of  $\lambda_a$  and  $K_2$  that are explicitly derived in the  $x < x_M$  case.  $C_o(\lambda_o, r_o)$  with  $r_o \equiv K_4 M / K_2 m_o$  is  $O(1)$ . Explicit formulas of the coefficients are given in Appendix C. There is another negative term with  $C_3$ , which is defined as follows:

$$C_3(r_o, \lambda_o, \lambda_n) = r_o \left[ \frac{\lambda_o - 1}{\lambda_o - 3} (k_{\min}^o)^{3-\lambda_o} + 2 \frac{B_o}{K_2} \langle (k^n) \rangle \langle (k^o)^2 \rangle + \left( \frac{B_o}{K_2} \right)^2 \langle (k^n)^2 \rangle \langle (k^o) \rangle \right]. \quad (\text{D25})$$

Note that this term does not appear in the original AT model defined on SF network.

We note that the  $C_o$  term is a leading order term at  $T_s$ , and  $C_o$  decreases monotonically with  $\lambda_o$ . Thus the sign of  $C_o$  can change depending on the magnitude of  $\lambda_o$ . This feature does not appear for both  $0 < x < x_M$  and  $x > x_M$  cases. However, it occurs when  $x = x_M$ . Numerically  $C_o = 0$  at  $\lambda_o \approx 3.503$ , equivalent to  $\lambda_c$  introduced earlier in Secs. II and III:  $C_o$  becomes positive for  $\lambda_o < \lambda_c$ , whereas it is negative for  $\lambda_o > \lambda_c$ . However,  $C_n$  and  $C_3$  are always positive and negative, respectively.

#### b. Case $\lambda_n = \lambda_o$

When  $\lambda_n = \lambda_o$ , the  $C_o$  and  $C_n$  terms in Eq. (D24) are of the same order. Thus, the two terms are combined and denoted as  $C'_o(\lambda_o, r_o)(K_2 m_o)^{\lambda_o-1}$ . The sign of  $C'_o$  depends on  $\lambda_o$ , equivalently  $\lambda_n$ . Numerically  $C'_o$  can be zero at a certain  $\lambda_o$ , denoted as  $\lambda_e$ , estimated to be  $\approx 3.605$ .  $C'_o$  becomes positive for  $\lambda_o < \lambda_e$  and negative otherwise.

Similar to the previous case  $\lambda_n > \lambda_o$ , a discontinuous transition always occurs for  $C'_o < 0$ . However, depending on relative magnitude between two terms  $C'_o$  and  $C_3$ , either a discontinuous or continuous transition occurs for  $C'_o > 0$ . Note that successive discontinuous transitions do not occur for  $\lambda_n = \lambda_o$ .

### c. Case $\lambda_n < \lambda_o$

When  $\lambda_n < \lambda_o$ ,  $O(m_a) \ll O(M)$ , the free-energy density of Eq. (18) is expanded with respect to  $m_n$  as follows:

$$f(m_n) \simeq f_0(M_*) + A'_n K_2 m_n^2 \left(1 - \frac{T_s}{T}\right) + C_n(\lambda_n)(K_2 m_n)^{\lambda_n-1} + C_o(\lambda_o)(B'_n m_n)^{\lambda_o-1} \\ - \frac{K_2[(\lambda_o - 1)C_o(\lambda_n)]^2}{\langle k_o \rangle [1 - ((k_o^2)/\langle k_o \rangle) + g_o(M_*)]/T]} (B'_n m_n)^{2(\lambda_o-2)} - \frac{1}{2}(\lambda_o - 3) \frac{K_4[D_M(\lambda_o)(K_4 M_*)^{\lambda_o-4}]^2}{\langle k_o \rangle (T_{s,M}/T - 1)} (B'_n m_n)^4 + \text{h.o.}$$

This formula is exactly the same as Eq. (D22), derived in  $x > x_M$  case for continuous transitions.

## APPENDIX E: THE SUSCEPTIBILITY NEAR THE CRITICAL TEMPERATURE

### 1. $m_a$ -magnetization

#### a. for $x \leq x_M$

Now, we consider the susceptibility at the critical temperature  $T_s$  for weak interlayer interaction  $x < x_M$  case. We can omit the higher-order terms in  $m_a$  and  $M$  when  $m_a$  and  $M$  are very small, we expand the self-consistency relations for  $m_a$  (A2) with respect to  $m_a$  and  $M$  as follows:

$$m_a \langle k_a \rangle \simeq \Omega_a \langle k_a^2 \rangle + \Omega_{\bar{a}} \langle k_o \rangle \langle k_n \rangle - (\lambda_a - 1) C_a(\lambda_a) (\Omega_a)^{\lambda_a-2}. \quad (\text{E1})$$

To obtain critical exponent  $\gamma$  for each  $m_a$ -magnetization, respectively, we consider the lowest-order terms of the self-consistency relations Eqs. (E1) and then we obtain the following:

$$m_a \langle k_n \rangle \langle k_o \rangle \left(1 - \frac{T_\ell}{T}\right) \left(1 - \frac{T_s}{T}\right) \simeq E_{\bar{a}} (H_a \langle k_a^2 \rangle + H_{\bar{a}} \langle k_o \rangle \langle k_n \rangle - (\lambda_a - 1) C_a(\lambda_a) (\Omega_a)^{\lambda_a-2}) \\ + F_{a\bar{a}} (H_{\bar{a}} \langle k_a^2 \rangle + H_a \langle k_a \rangle \langle k_{\bar{a}} \rangle - (\lambda_{\bar{a}} - 1) C_{\bar{a}}(\lambda_{\bar{a}}) (\Omega_{\bar{a}})^{\lambda_{\bar{a}}-2}) + \text{h.o.}, \quad (\text{E2})$$

where  $E_{\bar{a}} = \langle k_{\bar{a}} \rangle (1 - \frac{\langle k_{\bar{a}}^2 \rangle}{\langle k_{\bar{a}} \rangle})$  and  $F_{a\bar{a}} = \frac{1}{T} \langle k_o \rangle \langle k_n \rangle$ .

To derive the susceptibility from magnetization, we take partial derivative with respect to  $H_a$  and then take the  $H_a$  and  $H_{\bar{a}} \rightarrow 0$  limit. We have two equations for the susceptibility as follows:

$$\chi_a \langle k_a \rangle \langle k_{\bar{a}} \rangle \left(1 - \frac{T_\ell}{T}\right) \left(1 - \frac{T_s}{T}\right) \simeq E_{\bar{a}} (\langle k_a^2 \rangle - (\lambda_a - 1)(\lambda_a - 2) C_a(\lambda_a) (K_2 m_a)^{\lambda_a-3} K_2 \chi_a) \\ + F \left( \langle k_a \rangle \langle k_{\bar{a}} \rangle - (\lambda_{\bar{a}} - 1)(\lambda_{\bar{a}} - 2) C_{\bar{a}}(\lambda_{\bar{a}}) (K_2 m_{\bar{a}})^{\lambda_{\bar{a}}-3} K_2 \frac{\partial m_{\bar{a}}}{\partial H_a^2} \right) + \text{h.o.} \quad (\text{E3})$$

When  $\lambda_o < \lambda_n$ , the susceptibility near the critical temperature  $T_s^-$  is written as follows:

$$\chi_o \langle k_n \rangle \langle k_o \rangle \left(1 - \frac{T_\ell}{T}\right) \left(1 - \frac{T_s}{T}\right) \approx E_n \langle k_o^2 \rangle + F \langle k_o \rangle \langle k_n \rangle + (\lambda_o - 2) \langle k_o \rangle \langle k_n \rangle \left(1 - \frac{T_\ell}{T}\right) \left(1 - \frac{T_s}{T}\right) \chi_o + \text{h.o.}, \\ \chi_n \langle k_n \rangle \langle k_o \rangle \left(1 - \frac{T_\ell}{T}\right) \left(1 - \frac{T_s}{T}\right) \approx E_o \langle k_n^2 \rangle + F \langle k_o \rangle \langle k_n \rangle + (\lambda_o - 2) \langle k_o \rangle \langle k_n \rangle \left(1 - \frac{T_\ell}{T}\right) \left(1 - \frac{T_s}{T}\right) \frac{E_o}{E_n} \frac{\partial m_o}{\partial H_n} + \text{h.o.} \quad (\text{E4})$$

To obtain the susceptibility near  $T_s^-$ , we use the following relation:

$$E_n(-(\lambda_o - 1) K_2 C_o(\lambda_o) (K_2 m_o)^{\lambda_o-3}) \approx \langle k_o \rangle \langle k_n \rangle \left(1 - \frac{T_\ell}{T}\right) \left(1 - \frac{T_s}{T}\right) \quad \text{for } T \rightarrow T_s^-. \quad (\text{E5})$$

To get  $\chi_n$ , we need to compute the  $\partial m_o / \partial H_n$  term. The partial derivative of  $m_o$  in terms of  $H_n$  is given as follows:

$$\frac{\partial m_o}{\partial H_n} \langle k_o \rangle \langle k_n \rangle \left(1 - \frac{T_\ell}{T}\right) \left(1 - \frac{T_s}{T}\right) \simeq E_n \left( \langle k_o \rangle \langle k_n \rangle + (\lambda_o - 1)(\lambda_o - 2) C_o(\lambda_o) (K_2 m_o)^{\lambda_o-3} K_2 \frac{\partial m_o}{\partial H_n} \right) + F \langle k_n^2 \rangle + \text{h.o.} \\ \simeq E_n \langle k_o \rangle \langle k_n \rangle + F \langle k_n^2 \rangle + (\lambda_o - 2) \langle k_o \rangle \langle k_n \rangle \left(1 - \frac{T_\ell}{T}\right) \left(1 - \frac{T_s}{T}\right) \frac{\partial m_o}{\partial H_n} + \text{h.o.} \quad (\text{E6})$$

From Eq. (E6), we obtain that  $\partial m_o/\partial H_n \approx (T_s - T)^{-1}$  for  $T \rightarrow T_s^-$ . Using this, the susceptibility of  $m_a$  is obtained as

$$\chi_o \approx \begin{cases} (T - T_s)^{-1} & \text{for } T_s^+, \\ (T_s - T)^{-1} & \text{for } T_s^-, \end{cases} \quad \text{and} \quad \chi_n \approx \begin{cases} (T - T_s)^{-1} & \text{for } T_s^+, \\ (T_s - T)^{-1} & \text{for } T_s^-. \end{cases} \quad (\text{E7})$$

Here, we take the limit  $m_o \rightarrow 0$  for near  $T_s^+$  to Eq. (E3). For the  $\lambda_n < \lambda_o$  case, the susceptibility of  $m_a$  is obtained by similar computation process same as for the  $\lambda_o < \lambda_n$  case. Thus, the critical exponent of  $\gamma_{m\pm}$  of magnetization is always 1 for all cases. Then, the scaling relation,  $a + 2\beta_m + \gamma_{m-} = 2$ , is satisfied for each  $m_a$ -magnetization, respectively.

Now, we compute the susceptibility at CE point as boundary point of continuous PT regime. Since the location of magnetization jumps to a certain finite at the CE, the magnitude of the magnetization is much greater than 0, the perturbative expansions with respect to  $m, M$  is not valid any longer at CE point. Thus, we should keep the integral formula written in self-consistent relation Eqs. (A2) and (A3) as follows. To obtain the susceptibility for  $m_a$  magnetization, we take a partial derivative of self-consistent relation for  $m_a$  Eq. (A2) with respect of  $H_2$  and take  $H_2, H_4 \rightarrow 0$  limit, then the susceptibility is written as follows:

$$\chi_o = \frac{\mathcal{A}_{oo} + \mathcal{A}_{on}K_2\partial m_n/\partial H_o + \mathcal{A}_{oM}K_4\partial M/\partial H_o}{\langle k_o \rangle - K_2\mathcal{A}_{oo}}. \quad (\text{E8})$$

To evaluate Eq. (E8), we also should compute the

$$\left. \frac{\partial m_n}{\partial H_o} \right|_{H_a, H_4 \rightarrow 0} \quad \text{and} \quad \left. \frac{\partial M}{\partial H_o} \right|_{H_a, H_4 \rightarrow 0} \quad (\text{E9})$$

terms. Thus, we first take a derivative of self-consistent relation for  $m_n$  and  $M$  Eqs. (A2) and (A3) with respect to  $H_o$  and then take the limit  $H_a$  and  $H_4 \rightarrow 0$ , we obtain as follows:

$$\frac{\partial m_n}{\partial H_o} = \frac{\mathcal{A}_{no} + \mathcal{A}_{no}K_2\chi_o + \mathcal{A}_{nM}K_4\partial M/\partial H_o}{\langle k_n \rangle - K_2\mathcal{A}_{nn}}, \quad \frac{\partial M}{\partial H_o} = \frac{\mathcal{A}_{Mo} + \mathcal{A}_{Mo}K_2\chi_o + \mathcal{A}_{Mn}K_2\partial m_n/\partial H_o}{\langle k_o \rangle - K_4\mathcal{A}_{MM}}. \quad (\text{E10})$$

At the CE point,  $\chi_o$  is computed similarly to Eq. (E3) at  $T_s^+$ , where  $m_a = M = 0$ . For  $T_s^-$ ,  $\chi_m$  can be obtained numerically from Eqs. (E8) and (E10). We can confirm that the susceptibility has a certain finite value at  $T_s^-$  by numerical computations.

### b. Case $x > x_M$

Otherwise, for  $x > x_M$ , we expand the self-consistency relations for  $m_a$  with respect to  $m_a$  and  $M$  as follows:

$$m_a \langle k_n \rangle \langle k_o \rangle \left(1 - \frac{T'_\ell}{T}\right) \left(1 - \frac{T'_s}{T}\right) \simeq E'_a [H_a \langle k_a^2 \rangle + H_a \langle k_o \rangle \langle k_n \rangle - (\lambda_a - 1)C_a(\lambda_a)(\Omega_a)^{\lambda_a - 2}] \\ + F'_{aa} [H_a \langle k_a^2 \rangle + H_a \langle k_a \rangle \langle k_a \rangle - (\lambda_a - 1)C_a(\lambda_a)(\Omega_a)^{\lambda_a - 2}] + \text{h.o.}, \quad (\text{E11})$$

where  $E'_a = \langle k_a \rangle (1 - \frac{\langle k_a^2 \rangle / \langle k_a \rangle + g_a(M_a)}{T})$  and  $F'_{aa} = \frac{1}{T} \langle k_o \rangle \langle k_n \rangle + \frac{1}{T} K_4 M_* \langle k_o^2 \rangle \langle k_n \rangle$ .

It can be checked easily that Eq. (E11) is similar case to Eq. (E2) except the critical temperature  $T'_s$  and coefficients  $E'_a$  and  $F'$ . Thus, we performed similar calculations as for the  $x < x_M$  case considering minor differences between the cases  $x < x_M$  and  $x > x_M$ . By performing similar calculations as for the  $x < x_M$  case, we obtain the susceptibility of  $m_a$  as follows:

$$\chi_o \approx \begin{cases} (T - T'_s)^{-1} & \text{for } T > T'_s, \\ (T'_s - T)^{-1} & \text{for } T'_s > T, \end{cases} \quad \text{and} \quad \chi_n \approx \begin{cases} (T - T'_s)^{-1} & \text{for } T > T'_s, \\ (T'_s - T)^{-1} & \text{for } T'_s > T. \end{cases} \quad (\text{E12})$$

## 2. M-magnetization

Likewise, the self-consistency relation for  $M$  Eq. (A3) can be expanded as

$$M \langle k_o \rangle \simeq \Omega_4 \langle k_o^2 \rangle - (\lambda_o - 1)C_M(\lambda_o)\Omega_4^{\lambda_o - 2} - D_m(\lambda_o)\Omega_{\lambda_o - 2} + \text{h.o.} \quad (\text{E13})$$

To obtain the susceptibility of  $M$ , we take partial derivative of the above self-consistency relation with respect to  $H_4$  and then taking  $H_2$  and  $H_4 \rightarrow 0$ :

$$\chi_M \langle k_o \rangle \simeq (K_4 \chi_M + 1) \langle k_o^2 \rangle - (\lambda_o - 2)C_M(\lambda_o)(K_4 \chi_M)(K_4 M)^{\lambda_o - 3} - (\lambda_o - 2)D_m(\lambda_o)(K_2 m_o)^{\lambda_o - 3} K_2 \frac{\partial m_o}{\partial H_4} + \text{h.o.} \quad (\text{E14})$$

For  $x < x_M$ , because  $M$  is  $O(m_o^{\lambda_o - 2})$ ,  $\partial m_o/\partial H_4$  is very small compared with the  $O(1)$  term. Taking this limit, we obtain the susceptibility of  $M$ . We also take the limit  $m_o = 0$  for  $T_s^+$ :

$$\chi_M \approx \left( T - x \frac{\langle k_o^2 \rangle}{\langle k_o \rangle} \right)^{-1}. \quad (\text{E15})$$

Otherwise,  $x \geq x_M$  and  $T \rightarrow T_{s,M}^-$ ,  $M$  can be approximated to  $M_*$ , where  $M_*$  becomes Ising spin in single SF networks, and  $m_a$  is negligible to  $M$ . Taking this limit, we can obtain the susceptibility of  $M$  as follow. We also take the limit  $M = 0$  for  $T_{s,M}^+$ :

$$\chi_M \approx \begin{cases} (T - T_{s,M})^{-1} & \text{for } T > T_{s,M}, \\ (T_{s,M} - T)^{-1} & \text{for } T_{s,M} > T. \end{cases} \quad (\text{E16})$$

- 
- [1] A.-L. Barabási, *Network Science* (Cambridge University Press, Cambridge, UK, 2016).
- [2] S. N. Dorogovtsev, *Lectures on Complex Networks* (Oxford University Press, Oxford, UK, 2010).
- [3] M. E. J. Newman, *Networks: An Introduction* (Oxford University Press, Oxford, UK, 2010).
- [4] D. Lee, B. Kahng, Y. S. Cho, K.-I. Goh, and D.-S. Lee, *J. Korean Phys. Soc.* **73**, 152 (2018).
- [5] S. N. Dorogovtsev, A. V. Goltsev, and J. F. F. Mendes, *Rev. Mod. Phys.* **80**, 1275 (2008).
- [6] G. Bianconi, *Multilayer Networks: Structure and Function* (Oxford University Press, Oxford, UK, 2018).
- [7] S. V. Buldyrev, R. Parshani, G. Paul, H. E. Stanley, and S. Havlin, *Nature (London)* **464**, 1025 (2010).
- [8] S. Boccaletti, G. Bianconi, R. Criado, C. I. del Genio, J. Gómez-Gardeñes, M. Romance, I. Sendiña-Nadal, Z. Wang, and M. Zanin, *Phys. Rep.* **544**, 1 (2014).
- [9] M. Kivelä, A. Arenas, M. Barthelemy, J. P. Gleeson, Y. Moreno, and M. A. Porter, *J. Complex Netw.* **2**, 203 (2014).
- [10] K.-M. Lee, B. Min, and K.-I. Goh, *Eur. Phys. J. B* **88**, 48 (2015).
- [11] M. Szell, R. Lambiotte, and S. Thurner, *Proc. Natl. Acad. Sci. USA* **107**, 13636 (2010).
- [12] G. Menichetti, D. Remondini, P. Panzarasa, R. J. Mondragón, and G. Bianconi, *PLoS One* **9**, e97857 (2014).
- [13] A. Cardillo, J. Gómez-Gardeñes, M. Zanin, M. Romance, D. Papo, F. del Pozo, and S. Boccaletti, *Sci. Rep.* **3**, 1344 (2013).
- [14] E. Bullmore and O. Sporns, *Nat. Rev. Neurosci.* **10**, 186 (2009).
- [15] S. D. S. Reis, Y. Hu, A. Babino, J. S. Andrade Jr., S. Canals, M. Sigman, and H. A. Makse, *Nat. Phys.* **10**, 762 (2014).
- [16] G. Bianconi, *Phys. Rev. E* **87**, 062806 (2013).
- [17] B. Min, S. D. Yi, K.-M. Lee, and K.-I. Goh, *Phys. Rev. E* **89**, 042811 (2014).
- [18] V. Nicosia and V. Latora, *Phys. Rev. E* **92**, 032805 (2015).
- [19] H. Wu, R. G. James, and R. M. D'Souza, *J. Complex. Netw.* **8**, cnaa014 (2020).
- [20] G. J. Baxter, S. N. Dorogovtsev, A. V. Goltsev, and J. F. F. Mendes, *Phys. Rev. Lett.* **109**, 248701 (2012).
- [21] D. Cellai, E. Lopez, J. Zhou, J. P. Gleeson, and G. Bianconi, *Phys. Rev. E* **88**, 052811 (2013).
- [22] S. Hwang, S. Choi, D. Lee, and B. Kahng, *Phys. Rev. E* **91**, 022814 (2015).
- [23] G. Bianconi, S. N. Dorogovtsev, and J. F. F. Mendes, *Phys. Rev. E* **91**, 012804 (2015).
- [24] D. Cellai, S. N. Dorogovtsev, and G. Bianconi, *Phys. Rev. E* **94**, 032301 (2016).
- [25] S. Gómez, A. Díaz-Guilera, J. Gómez-Gardeñes, C. J. Pérez-Vicente, Y. Moreno, and A. Arenas, *Phys. Rev. Lett.* **110**, 028701 (2013).
- [26] M. De Domenico, A. Solé-Ribalta, S. Gómez, and A. Arenas, *Proc. Natl. Acad. Sci. USA* **111**, 8351 (2014).
- [27] A. Saumell-Mendiola, M. A. Serrano, and M. Boguna, *Phys. Rev. E* **86**, 026106 (2012).
- [28] E. Cozzo, R. A. Banos, S. Meloni, and Y. Moreno, *Phys. Rev. E* **88**, 050801(R) (2013).
- [29] C. Granell, S. Gómez, and A. Arenas, *Phys. Rev. Lett.* **111**, 128701 (2013).
- [30] Z. Wang, L. Wang, A. Szolnoki, and M. Perc, *Eur. Phys. J. B* **88**, 124 (2015).
- [31] M. Perc, J. Gómez-Gardeñes, A. Szolnoki, L. M. Floría, and Y. Moreno, *J. R. Soc. Interface* **10**, 20120997 (2013).
- [32] N. Masuda, *Phys. Rev. E* **90**, 012802 (2014).
- [33] M. Diakonova, M. San Miguel, and V. M. Eguíluz, *Phys. Rev. E* **89**, 062818 (2014).
- [34] M. Diakonova, V. Nicosia, V. Latora, and M. San Miguel, *New J. Phys.* **18**, 023010 (2016).
- [35] A. Chmiel and K. Sznajd-Weron, *Phys. Rev. E* **92**, 052812 (2015).
- [36] A. Chmiel, J. Sienkiewicz, A. Fronczak, and P. Fronczak, *Entropy* **22**, 1018 (2020).
- [37] A. Halu, K. Zhao, A. Baronchelli, and G. Bianconi, *Europhys. Lett.* **102**, 16002 (2013).
- [38] F. Battiston, A. Cairoli, V. Nicosia, A. Baule, and V. Latora, *Physica D* **323–324**, 12 (2016).
- [39] J. Ashkin and E. Teller, *Phys. Rev.* **64**, 178 (1943).
- [40] S. Jang, J. S. Lee, S. Hwang, and B. Kahng, *Phys. Rev. E* **92**, 022110 (2015).
- [41] R. V. Ditzian and L. P. Kadanoff, *J. Phys. A* **12**, L229 (1979).
- [42] F. Iglói and L. Turban, *Phys. Rev. E* **66**, 036140 (2002).
- [43] S. N. Dorogovtsev, A. V. Goltsev, and J. F. F. Mendes, *Eur. Phys. J. B* **38**, 177 (2004).
- [44] S. H. Lee, M. Ha, H. Jeong, J. D. Noh, and H. Park, *Phys. Rev. E* **80**, 051127 (2009).
- [45] F. Battiston, G. Cencetti, I. Iacopini, V. Latora, M. Lucas, A. Patania, J. G. Young, and G. Petri, *Phys. Rep.* **874**, 1-92 (2020).
- [46] G. Bianconi, *Higher-order Networks: An Introduction to Simplified Complexes* (Cambridge University Press, Cambridge, UK, 2021).